



DEGREE PROJECT IN ELECTRICAL ENGINEERING,
SECOND CYCLE, 30 CREDITS
STOCKHOLM, SWEDEN 2020

Implementation of an Arc Model for MV Network with Resonance Earthing

MUHANNAD ALMULLA

Implementation of an Arc Model for MV Network with Resonance Earthing

MUHANNAD ALMULLA

Master in Electrical Power Engineer

Date: February 27, 2020

Supervisor: Nathaniel Taylor, Zakaria Habib

Examiner: Hans Edin

School of Electrical Engineering and Computer Science

Swedish title: Implementering av en bågmodell för
mellanspänningssnät med resonansjordning

Abstract

The most common fault type in electric power systems is the line to ground fault. In this type of faults, an electrical arc is usually developed. The thesis presents a mathematical model that describes the behavior of the arc during a fault. The arc model has been verified based on real and simulated tests that were conducted on a system that has resonant earthing coil.

In addition, two studies have been conducted on the same verified system. The first studied was implemented to see the effect of detuning the resonant earthing coil at different levels. It was noted that detuning the coil affected AC and the DC components in the arc faults. Also, the detuning affected the arc extinction.

The second study has been looking at the effects of implementing a parallel resistor to the resonant earthing coil. The tests have been conducted using different set values of the resistor. In some of the studied cases and during the testing period, the resistor has affected the self-extinguish behavior of the arc.

Keywords

Distribution system, electrical arc, high impedance fault, Petersen coil, resonance earth.

Sammanfattning

Den vanligaste feltypen i elektriska kraftsystem är fas till jord. I denna typ av fel utvecklas vanligtvis en elektrisk ljusbåge. Examensarbetet presenterar en matematisk modell som beskriver ljusbågens beteende under ett fel. Bägmodellen har verifierats baserat på verkliga tester och simuleringar som utfördes på ett system som har resonansjordningsspole.

Dessutom har två studier genomförts på samma verifierade system. Den första studien genomfördes för att se effekten av avstämning av den resonanta jordningsspolen på olika nivåer. Det noterades att avstämning av spolen påverkade AC och DC-komponenterna i ljusbågsfel. Avstämningen påverkade också ljusbågens släckning.

Den andra studien har tittat på effekterna av att implementera ett parallellt motstånd till den resonanta jordningsspolen. Testen har utförts med olika inställda värden på motståndet. I några av de studerade fallen och under testperioden har motståndet påverkat ljusbågens självsläckande beteende.

Abbreviations and Notation

AC	Alternating Current
ATP-EMTP	Alternative Transients Program of ElectroMagnetic Transients Program
DC	Direct Current
EPS	Electrical Power Supply
HIF	High Impedance Fault
MV	Medium Voltage
TACS	Transient Analysis of Control System

Contents

1	Introduction	1
1.1	Background	1
1.2	Thesis Aims	2
1.3	Thesis Outline	2
2	Literature Review	4
2.1	Modelling the Arc Fault	4
2.1.1	Circuit Breaker Arc Models	4
2.1.1.1	Cassie-Mayr Method	4
2.1.1.2	Habedank Arc Model	5
2.1.1.3	Schwarz Arc Model	6
2.1.1.4	KEMA Arc Model	6
2.1.2	Line Fault Arc Models	9
2.1.2.1	HIF Models	9
2.1.2.2	Models Based on the Arc Energy Balance Column	13
2.2	Modeling Petersen Coil System	15
2.2.1	Background on Earthing System	15
2.2.2	Petersen Coil System Description	16
2.2.3	Implementing a Parallel Resistor to Petersen Coil Grounding System	17
3	Methodology of Modelling the Arc	19
3.1	Simulation Software	19
3.2	Arc Models	20
3.2.1	The Implementation of the First Arc Model	20
3.2.2	The Implementation of the Second Arc Model	22
3.2.3	Implemented Model in the Study	22
3.3	Testing System	24
4	Simulation Work and the Study Interests	26

4.1	ATP-EMTP Representation and Arc Model Implementation	26
4.2	Studying the Effect of Petersen Coil	30
4.3	Studying the Effect of Petersen Coil Parallel Resistor	30
5	Simulation Results	32
5.1	Initial Arc Model Implementation Results	32
5.1.1	Fault Inception at Voltage Maximum	33
5.1.2	Fault Inception at Voltage Zero-Crossing	35
5.2	Results from Detuning Petersen Coil at Different Degrees	37
5.2.1	Fault Inception at Voltage Maximum	37
5.2.1.1	Arc Voltage Measurements	37
5.2.1.2	Arc Current Measurements	40
5.2.2	Fault Inception at Voltage Crossing Zero	42
5.2.2.1	Arc Voltage Measurements	42
5.2.2.2	Arc Current Measurements	45
5.3	Results When Adding a Parallel Ground Resistor	48
5.3.1	Fault Inception at Voltage Maximum	48
5.3.1.1	Arc Voltage Measurements	48
5.3.1.2	Arc Current Measurements	51
5.3.2	Fault Inception at Voltage Crossing Zero	53
5.3.2.1	Arc Voltage Measurements	53
5.3.2.2	Arc current Measurements	56
6	Discussion Based on Simulation Results	59
6.1	Arc Model Implementation Test	59
6.2	The Effect of Detuning Petersen Coil Between -20% to +20%	59
6.3	The Effect of Implementing a Parallel Grounding Resistor	60
7	Conclusion	61
	Bibliography	62

List of Figures

2.1	Emanuel arc model, 1990 [6, 7]	9
2.2	HIF arc model, 1993 [7, 9]	10
2.3	HIF model with TACS, 1998 [7, 10]	10
2.4	HIF simplified model, 2003 [7, 11]	11
2.5	HIF simplified model, 2004 [7, 12]	11
2.6	HIF model with time controlled variable resistor, 2005 [7, 13]	12
2.7	HIF model by combining multiple Emanuel model, 2010 [7]	12
2.8	Star system with neutral connection [18]	15
2.9	Electrical network with a Petersen coil [18]	16
2.10	Petersen coil with parallel resistor [19]	17
3.1	The implementation of Thevenin method [14]	20
3.2	The implementation of iterated method [14]	21
3.3	The block diagram of the second arc model [2]	22
3.4	Arc fault model with dynamic controlled resistance [21] . .	23
3.5	The dynamic model code [21]	23
3.6	Testing system diagram [14]	24
4.1	System model in ATP-EMTP	27
4.2	The arc fault model code	28
4.3	Fault scenarios	28
4.4	MODEL component in ATP-EMTP	29
4.5	Implemented fault time in ATP-EMTP	29
4.6	System model with a parallel grounding resistor	31
5.1	Simulated vs expected fault voltage when fault inception at voltage maximum	33
5.2	Simulated vs expected fault current when fault inception at voltage maximum	33
5.3	Simulated vs expected Petersen coil current when fault inception at voltage maximum	33

5.4	Simulated arc length when fault inception at voltage maximum	33
5.5	Simulated arc resistance when fault inception at voltage maximum	34
5.6	Simulated stationary arc voltage when fault inception at voltage maximum	34
5.7	Simulated arc time constant when fault inception at voltage maximum	34
5.8	Simulated vs expected fault voltage when fault inception at voltage zero-crossing	35
5.9	Simulated vs expected fault current when fault inception at voltage zero-crossing	35
5.10	Simulated vs expected Petersen coil current when fault inception at voltage zero-crossing	35
5.11	Simulated arc length when fault inception at voltage zero-crossing	35
5.12	Simulated arc resistance when fault inception at voltage zero-crossing	36
5.13	Simulated stationary arc voltage when fault inception at voltage zero-crossing	36
5.14	Simulated arc time constant when fault inception at voltage zero-crossing	36
5.15	Fault voltage when detuning degree at -20% and fault inception at voltage maximum	37
5.16	Fault voltage when detuning degree at -15% and fault inception at voltage maximum	37
5.17	Fault voltage when detuning degree at -10% and fault inception at voltage maximum	38
5.18	Fault voltage when detuning degree at -5% and fault inception at voltage maximum	38
5.19	Fault voltage when detuning degree at 0% and fault inception at voltage maximum	38
5.20	Fault voltage when detuning degree at +5% and fault inception at voltage maximum	38
5.21	Fault voltage when detuning degree at +10% and fault inception at voltage maximum	39
5.22	Fault voltage when detuning degree at +15% and fault inception at voltage maximum	39

x LIST OF FIGURES

5.23	Fault voltage when detuning degree at +20% and fault inception at voltage maximum	39
5.24	Fault current when detuning degree at -20% and fault inception at voltage maximum	40
5.25	Fault current when detuning degree at -15% and fault inception at voltage maximum	40
5.26	Fault current when detuning degree at -10% and fault inception at voltage maximum	40
5.27	Fault current when detuning degree at -5% and fault inception at voltage maximum	40
5.28	Fault current when detuning degree at 0% and fault inception at voltage maximum	41
5.29	Fault current when detuning degree at +5% and fault inception at voltage maximum	41
5.30	Fault current when detuning degree at +10% and fault inception at voltage maximum	41
5.31	Fault current when detuning degree at +15% and fault inception at voltage maximum	41
5.32	Fault current when detuning degree at +20% and fault inception at voltage maximum	42
5.33	Fault voltage when detuning degree at -20% and fault inception at voltage zero-crossing	42
5.34	Fault voltage when detuning degree at -15% and fault inception at voltage zero-crossing	42
5.35	Fault voltage when detuning degree at -10% and fault inception at voltage zero-crossing	43
5.36	Fault voltage when detuning degree at -5% and fault inception at voltage zero-crossing	43
5.37	Fault voltage when detuning degree at 0% and fault inception at voltage zero-crossing	43
5.38	Fault voltage when detuning degree at +5% and fault inception at voltage zero-crossing	43
5.39	Fault voltage when detuning degree at +10% and fault inception at voltage zero-crossing	44
5.40	Fault voltage when detuning degree at +15% and fault inception at voltage zero-crossing	44
5.41	Fault voltage when detuning degree at +20% and fault inception at voltage zero-crossing	44

5.42	Fault current when detuning degree at -20% and fault inception at voltage zero-crossing	45
5.43	Fault current when detuning degree at -15% and fault inception at voltage zero-crossing	45
5.44	Fault current when detuning degree at -10% and fault inception at voltage zero-crossing	45
5.45	Fault current when detuning degree at -5% and fault inception at voltage zero-crossing	45
5.46	Fault current when detuning degree at 0% and fault inception at voltage zero-crossing	46
5.47	Fault current when detuning degree at +5% and fault inception at voltage zero-crossing	46
5.48	Fault current when detuning degree at +10% and fault inception at voltage zero-crossing	46
5.49	Fault current when detuning degree at +15% and fault inception at voltage zero-crossing	46
5.50	Fault current when detuning degree at +20% and fault inception at voltage zero-crossing	47
5.51	Fault voltages when detuning degree at -20% and fault inception at voltage maximum	48
5.52	Fault voltages when detuning degree at -15% and fault inception at voltage maximum	48
5.53	Fault voltages when detuning degree at -10% and fault inception at voltage maximum	49
5.54	Fault voltages when detuning degree at -5% and fault inception at voltage maximum	49
5.55	Fault voltages when detuning degree at 0% and fault inception at voltage maximum	49
5.56	Fault voltages when detuning degree at +5% and fault inception at voltage maximum	49
5.57	Fault voltages when detuning degree at +10% and fault inception at voltage maximum	50
5.58	Fault voltages when detuning degree at +15% and fault inception at voltage maximum	50
5.59	Fault voltages when detuning degree at +20% and fault inception at voltage maximum	50
5.60	Fault currents when detuning degree at -20% and fault inception at voltage maximum	51

5.61	Fault currents when detuning degree at -15% and fault inception at voltage maximum	51
5.62	Fault currents when detuning degree at -10% and fault inception at voltage maximum	51
5.63	Fault currents when detuning degree at -5% and fault inception at voltage maximum	51
5.64	Fault currents when detuning degree at 0% and fault inception at voltage maximum	52
5.65	Fault currents when detuning degree at +5% and fault inception at voltage maximum	52
5.66	Fault currents when detuning degree at +10% and fault inception at voltage maximum	52
5.67	Fault currents when detuning degree at +15% and fault inception at voltage maximum	52
5.68	Fault currents when detuning degree at +20% and fault inception at voltage maximum	53
5.69	Fault voltages when detuning degree at -20% and fault inception at voltage zero-crossing	53
5.70	Fault voltages when detuning degree at -15% and fault inception at voltage zero-crossing	53
5.71	Fault voltages when detuning degree at -10% and fault inception at voltage zero-crossing	54
5.72	Fault voltages when detuning degree at -5% and fault inception at voltage zero-crossing	54
5.73	Fault voltages when detuning degree at 0% and fault inception at voltage zero-crossing	54
5.74	Fault voltages when detuning degree at +5% and fault inception at voltage zero-crossing	54
5.75	Fault voltages when detuning degree at +10% and fault inception at voltage zero-crossing	55
5.76	Fault voltages when detuning degree at +15% and fault inception at voltage zero-crossing	55
5.77	Fault voltages when detuning degree at +20% and fault inception at voltage zero-crossing	55
5.78	Fault currents when detuning degree at -20% and fault inception at voltage zero-crossing	56
5.79	Fault currents when detuning degree at -15% and fault inception at voltage zero-crossing	56

5.80	Fault currents when detuning degree at -10% and fault inception at voltage zero-crossing	56
5.81	Fault currents when detuning degree at -5% and fault inception at voltage zero-crossing	56
5.82	Fault currents when detuning degree at 0% and fault inception at voltage zero-crossing	57
5.83	Fault currents when detuning degree at +5% and fault inception at voltage zero-crossing	57
5.84	Fault currents when detuning degree at +10% and fault inception at voltage zero-crossing	57
5.85	Fault currents when detuning degree at +15% and fault inception at voltage zero-crossing	57
5.86	Fault currents when detuning degree at +20% and fault inception at voltage zero-crossing	58

List of Tables

4.1	The studied Petersen coil detuning levels	30
4.2	Values of Petersen coil parallel resistor used in the study . . .	30

Chapter 1

Introduction

The first chapter will cover some background information related to the thesis topic and it will also present the thesis aims.

1.1 Background

Single line to ground fault is the most common fault type in electric power systems. This type of fault is initiated by having a single phase of the electric power-lines in contact with a grounding point that causes a short circuit. The two contact points do not need to be in a direct connection. The fault can still occur if there is an air gap that is small enough to initiate a ground fault through an electric arc. The size of the gap depends on several factors, such as the voltage level of the energized contact. Other factors are the characteristics of the air in the gap between the two connection points. In most cases, a system that has arc suppression coils, the arc fault will automatically be cleared after a while [1].

Researches on finding a model that represents an electric arc go back to 1930, where the first mathematical models were designed to mimic the circuit breaker arcs that appear during the opening and the closing of the breaker. These models were first introduced by both Mayr and Cassie. Other circuit break arc models have later been developed using the approach of Mayr and Cassie. While this thesis aims to model the arc faults through the air and not the arc that is developed by the circuit breaker, several circuit breaker arc models are presented in Chapter 2 as part of the arc model development history.

The first mathematical equation of the arc fault was introduced by *Hochrainer* in 1971. This equation is based on the energy balance of the arc column. Several researchers have used *Hochrainer's* equation to build a model that represents the arc faults. Some of these models are described in Chapter 2, while one of these models was then chosen to be implemented in this thesis.

1.2 Thesis Aims

There is a lack of research in this field, which is one of the challenges in this thesis. Also, one of the barriers that face the MV distribution networks is the design of the electrical power system protection. MV distribution networks typically have a high ground impedance which reduces the amplitude of the returned ground current that is measured by the protection devices at the substation side. In some cases where there is a fault due to a fallen power-line, the ground fault can be very small and not being detected by the protection system. Arc fault models can help in improving the system protection with a better logic that can precisely identify an arc when it occurs in these types of faults. Ultimately, this will help in shaping the design and the standards of the electrical power equipment.

This thesis aims to implement an accurate model that represents the arc faults in MV networks with resonance earthing system. Subsequently, the model is going to be used to conduct two studies. The first study is on the effect of detuning the inductance value of the resonance earth coils. The second study is to see how the arc fault behaves when implementing a parallel grounding resistor at different set values.

1.3 Thesis Outline

Including this introductory chapter, there are a total of seven chapters in this thesis. The six upcoming chapters are listed below with a brief description of their respective content:

Chapter 2 Several arc models are presented in this chapter with their descriptions. In this thesis, the arc models are divided into two types, the first type is for circuit breaker arc models while the second type is related to line arc faults. Also, the chapter describes the resonance earth grounding system and two styles of its implementations.

Chapter 3 The chapter presents the methodology behind the conducted study. Information on ATP-EMTP, which is the software tool that was used to simulate the system. Three approaches to model electrical arc faults are provided in this chapter. One of the three models is implemented and used in the study, while the other two models are the basis from which the implemented model is derived. Also, the chapter exhibits the testing network and its parameters that were used during the study.

Chapter 4 This chapter shows the reflection of the selected arc model and the whole testing network in ATP-EMTP. The chapter also presents the three tests that were conducted in this thesis. The first test was implemented to confirm the arc model functionality. The second test was implemented to study the effect on the system voltage and current when the detuning degree of the Petersen coils are being set at various impedance values. The third test was conducted to analyze the behavior of the system voltage and current when adding a parallel ground resistor at different resistance values.

Chapter 5 The results of the three conducted studies are presented in this chapter. The results are provided in graphs that show the system's fault voltage and current in each of the conducted scenarios.

Chapter 6 The outcomes of the system implementation test and the two performed studies are individually presented and discussed in the chapter in detail.

Chapter 7 The chapter summarizes the thesis work and presents the main results outcomes.

Chapter 2

Literature Review

The main goal of the literature review is to structure a method to implement the arc fault in the MV power network that has resonance earth system.

The work has been divided into two segments:

1. Methods of implementing the arc fault
2. Methods of implementing the resonance earthing

2.1 Modelling the Arc Fault

Several models have been introduced to represent the arc. Most of these models depend on the rules of the thermal equilibrium, as it helps in modeling the arc's dynamics. These arc models have been designed to be used for either modeling the circuit breaker arcs or modeling arcing faults [2]. Although the focus of this thesis is to find models that are used for the arcing faults, an overview of the other methods will be provided.

2.1.1 Circuit Breaker Arc Models

2.1.1.1 Cassie-Mayr Method

A.M. Cassie and O. Mayr conducted their first experiments on electric arc in 1930. Mayr's equation is considered as the most used method for studying the dynamic behavior of the electrical arc. Mayr's and Cassie's equations are considered as the basis of several models that were invented afterwards [3, 4].

$$\frac{1}{G} \cdot \frac{dG}{dt} = \frac{1}{\tau_m} \left(\frac{u \cdot i}{P_0} - 1 \right) \quad (2.1)$$

Mayr's model is represented in equation (2.1), where: u is the instant value of the arc voltage, i is instant value of the arc current, G is the dynamic conductance of the electric arc, τ_m is the time constant of the electric arc at current zero moment, and P_0 is a constant value that represents the cooling power at current passing through zero.

$$\frac{1}{G} \cdot \frac{dG}{dt} = \frac{1}{\tau_c} \left(\frac{u^2}{U_a^2} - 1 \right) \quad (2.2)$$

Cassie's model is represented in equation (2.2), where: u is the instant value of the arc voltage, G is the dynamic conductance of the electric arc, τ_c is the time constant of the electric arc at the maximum current value, and U_a is a constant value that represents the electric arc voltage.

Although both Mayr and Cassie arc models are used for investigating the dynamic regime of an electrical arc, Mayr's equation is usually used for an electrical arc that is in the range of current passing through zero. While Cassie's equation is typically used for an electrical arc that is in the range of high-current phase.

2.1.1.2 Habedank Arc Model

Habedank model utilizes the structural equation of both Cassie and Mayr arc models. Habedank model includes the conductance from Cassie's equation in the form of G_c with the following formula [3, 5]:

$$G_c = \frac{i}{u_c} \quad (2.3)$$

It also includes the conductivity from Mayr's equation in the form of G_m with the following formula:

$$G_m = \frac{i}{u_m} \quad (2.4)$$

Habedank's model has three unknowns: G_c , G_m , and G , where G is the electrical arc conductance that is calculated by:

$$G = \frac{i}{u} \quad (2.5)$$

In the end, Habedank model is as the following:

$$\frac{dG_c}{dt} = \frac{G_c}{\tau_c} \left[\frac{u^2}{U_a^2} \cdot \left(\frac{G}{G_c} \right)^2 - 1 \right] \quad (2.6)$$

$$\frac{dG_m}{dt} = \frac{G_m}{\tau_m} \left(\frac{u^2 G}{P_m} \cdot \frac{G}{G_m} - 1 \right) \quad (2.7)$$

$$\frac{1}{G} = \frac{1}{G_c} + \frac{1}{G_m} \quad (2.8)$$

where the aforementioned parameters have the following physical meanings:

G_c : Cassie components of the arc conductance

G_m : Mayr components of the arc conductance

τ_c : Cassie time constant

U_a : steady-state voltage

τ_m : Mayr time constant

P_m : cooling power

2.1.1.3 Schwarz Arc Model

Schwarz has modified Mayr arc model by having the arc parameters depend on the arc conductance. Schwarz arc model presents the arc time constant τ_m and the arc cooling power P_0 in the form of power functions. The arc cooling power is presented as $P_0 = B \cdot G^\beta$, while the arc time constant is presented as $\tau_m = A \cdot G^\alpha$. The final model is expressed as the following [3, 5]:

$$\frac{1}{G} \cdot \frac{dG}{dt} = \frac{1}{A \cdot G^\alpha} \left(\frac{u \cdot i}{B \cdot G^\beta} - 1 \right) \quad (2.9)$$

where the parameters in equation (2.9) have the following physical meanings:

A : the arc time constant-coefficient and has the dimension of $s \cdot \Omega^\alpha$

α : the arc time constant exponent of the conductance

B : the arc cooling power constant and has the dimension of $W \cdot \Omega^\beta$

β : the arc cooling power exponent of the conductance

2.1.1.4 KEMA Arc Model

KEMA arc model gives a representation of the arc voltage before current zero region. KEMA model combines three sub-modules in series and it is on the

classical arc model concept. The model can be presented mathematically as the followings [5]:

$$\frac{dg_1}{dt} = \frac{u_1^2 g_1^2}{T_1 P_1} - \frac{g_1}{T_1} \quad (2.10)$$

$$\frac{dg_2}{dt} = \frac{u_2^2 g_2^2}{T_2 P_2} - \frac{g_2}{T_2} \quad (2.11)$$

$$\frac{dg_3}{dt} = \frac{u_3^2 g_3^2}{T_3 P_3} - \frac{g_3}{T_3} \quad (2.12)$$

$$P_1 = B_1 g_1^{0.6} \quad (2.13)$$

$$P_2 = B_2 g_2^{0.1} \quad (2.14)$$

$$\frac{1}{g} = \frac{1}{g_1} + \frac{1}{g_2} + \frac{1}{g_3} \quad (2.15)$$

$$u = u_1 + u_2 + u_3 \quad (2.16)$$

where g_1 , g_2 , and g_3 represent the arc conductance and u_1 , u_2 , and u_3 represent the arc voltage. The arc model also has six parameters which are:

T_1 , T_2 , and T_3 : time constants

B_1 and B_2 : cooling power parameters

P_3 : cooling power

The principle behind equation (2.10) and (2.11) is from the Schwarz arc model with fixed time constant, while equation (2.12) is based on the Mayr arc model. Equation (2.10) and (2.11) have the cooling powers which are defined by the arc conductance as shown in (2.13) and (2.14).

Although the model has several parameters, they are interconnected via the following relationships:

$$T_2 = \frac{T_1}{k_1} \quad (2.17)$$

$$T_3 = \frac{T_2}{k_2} \quad (2.18)$$

$$P_3 = \frac{B_2}{k_3} \quad (2.19)$$

where, k_1 and k_2 are constants that depend on the design of the circuit breaker (dimensionless). k_3 is also a constant that also depends on the design of the circuit breaker ($\Omega^{0.1}$)

k_1 , k_2 , and k_3 have an average value of 5.3, 5.8, and 113 ($\Omega^{0.1}$) respectively. These values have been obtained after several hundred short-circuit tests with a rated voltage between 72.5-550 kV, which included over 30 circuit breakers of different designs.

This concludes that the only parameters that will be changing from test to another are: T_1 , B_1 , and B_2 .

2.1.2 Line Fault Arc Models

The main objective of the thesis is to implement an arc fault model that can accurately represent line arc faults in MV networks with the resonant earthing system. To model the line arcing fault, two schools of thought have been studied. The first school of thought is focusing on the behavior of the high impedance fault (HIF) and it is started back in 1990 [6]. The second group relies on *Hochrainer* equation that is based on the arc energy balance column [1]. Both of these groups are going to be discussed in details in the following sections.

2.1.2.1 HIF Models

HIF is the act at which an overhead line or power cable disconnects and touches a high impedance surface such as a tree, a road, or a sandy ground. Since the fault is going through a high impedance point, the fault current will not change to a value that can be sensed by the over-current protection relays [7, 8]. For that reason, researchers have tried to study the HIFs by looking into the current harmonics [6]. In addition, HIF models usually include the arcing characteristic that occurs in this type of faults [7, 8].

A. Emanuel Model, 1990

Figure 2.1 represents a circuit model presented by Emanuel in 1990, which is based on several laboratory measurements. The model contains two diodes and two DC sources that represent a minimum threshold and only allow the current in the positive half cycle to pass when the voltage V_A is higher than V_p . Similarly, the negative half cycle current will only pass when the voltage V_A is higher than V_n [6, 7].

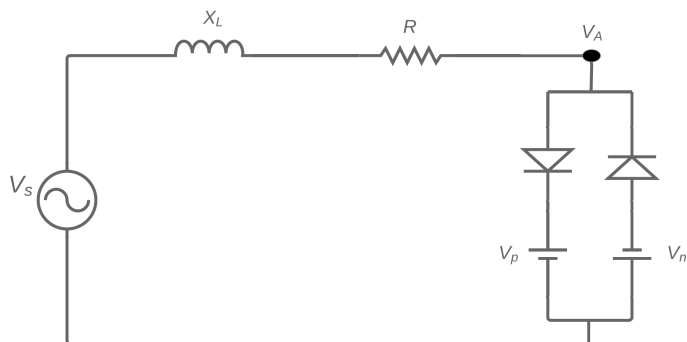


Figure 2.1: Emanuel arc model, 1990 [6, 7]

B. HIF Model in 1993

In 1993, an arc model has been implemented based on Emanuel's outcomes. The model tries to include the nonlinearity behavior of HIF. This has been achieved by replacing the DC voltage sources in the previous model with variable resistors [7, 9]. The model is presented in figure 2.2.

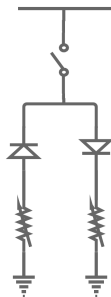


Figure 2.2: HIF arc model, 1993 [7, 9]

C. HIF Model with Transient Analysis of Control System, 1998

Figure 2.3 illustrates a 1998 HIF model with a transient analysis of control system (TACS) along with a varying resistor and two AC voltage sources [7, 10].

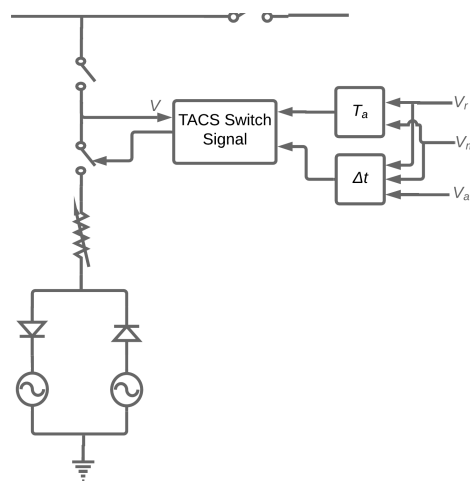


Figure 2.3: HIF model with TACS, 1998 [7, 10]

D. Simplified Emanuel Model, 2003

In 2003, a simplified model that added two resistors where each of them

is in series with the DC voltage sources that are in Emanuel original model. These resistors represent the asymmetric component of the fault currents [7, 11]. The model is presented in figure 2.4.

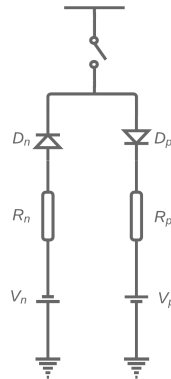


Figure 2.4: HIF simplified model, 2003 [7, 11]

E. Another Simplified HIF Model, 2004

This model which came in 2004 has a nonlinear resistor that is in series with two diodes and two DC voltage sources. The two DC voltage sources randomly change their amplitudes in every half cycle [7, 12]. The model is presented in figure 2.5.

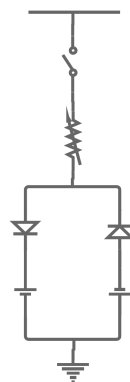


Figure 2.5: HIF simplified model, 2004 [7, 12]

F. HIF Model with Time Controlled Variable Resistor, 2005

This model has introduced the ideas of *Hochrainer* on the arc energy balanced column into a HIF model in terms of a time-varying controlled resistor. In addition, the model has DC and AC voltage sources and two

diodes with polarizing ramp voltages that are controlling the arc ignition instants [1, 7, 13, 14]. The model is presented in figure 2.6.

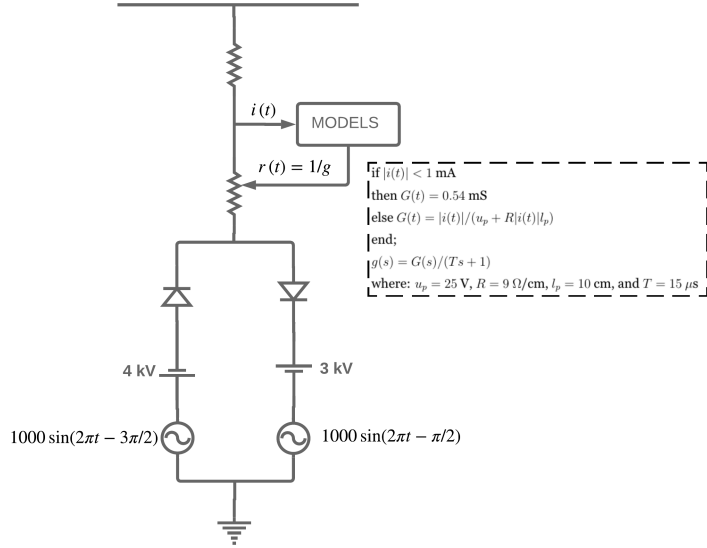


Figure 2.6: HIF model with time controlled variable resistor, 2005 [7, 13]

G. HIF Model by Combining Multiple Emanuel Model, 2010

This model has been introduced in 2010. The model uses a combination of several Emanuel models in parallel with each other where each line is controlled by a switch. This will avoid the changing of the model arc parameters by having a fixed value of each component and defining the switching time of each line [7]. Figure 2.7 gives an illustration of the model.

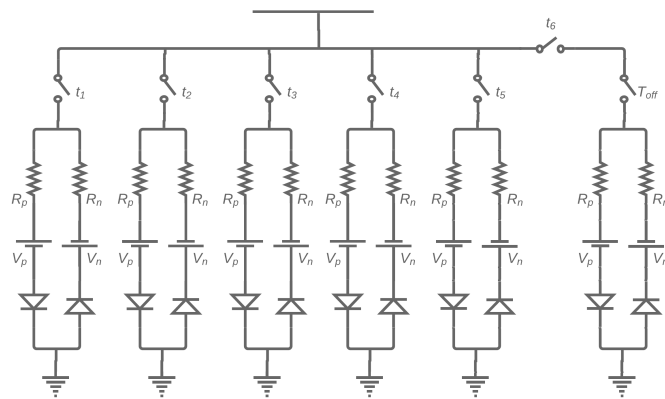


Figure 2.7: HIF model by combining multiple Emanuel model, 2010 [7]

2.1.2.2 Models Based on the Arc Energy Balance Column

These models use differential equations to calculate long arc in the air. It started with the work of *Hochrainer* in 1971 [1]. The arc conductance g has been described using the following differential equation [1, 14–16]:

$$\frac{dg}{dt} = \frac{1}{\tau} (G - g) \quad (2.20)$$

where the introduced parameters has the following physical meanings:

τ : The arc time constant

g : Instantaneous arc conductance

G : Stationary arc conductance

Equation (2.20) has two variables that need to be calculated, which are G and τ . Two ways of finding the values of both of these variables are going to be presented. One is described by [14]. The other method is presented by [2].

A. First Method of Finding G and τ

To calculate the arc time constant τ , equation (2.21) has been introduced [14].

$$\tau = \tau_0 \cdot \left(\frac{l_{arc}}{l_0} \right)^{-\alpha} \quad (2.21)$$

where, τ_0 is the initial time constant, l_0 is the initial arc length, α is a coefficient with a value between 0.1 to 0.6 [17], and l_{arc} is the time-varying arc length which is also called the arc elongation. τ_0 , l_0 , and α are representing the arc characteristic and their values vary depending on the system.

The stationary arc conductance G can be found using equations (2.22) - (2.25).

$$G = \frac{|i_{arc}|}{u_{st}} \quad (2.22)$$

$$u_{st} = u_0 + r_0 \cdot |i_{arc}| \quad (2.23)$$

$$u_0 = 0.9 \frac{\text{kV}}{\text{m}} \cdot l_{arc} + 0.4 \text{ kV} \quad (2.24)$$

$$r_0 = 40 \frac{\text{m}\Omega}{\text{m}} \cdot l_{arc} + 8 \text{ m}\Omega \quad (2.25)$$

where i_{arc} is the instantaneous arc current, u_{st} is the stationary arc voltage, u_0 is the characteristic arc voltage, and r_0 is the characteristic arc resistance. Equations (2.21), (2.24) and (2.25) show the effect of the arc length l_{arc} on the system. It is difficult to predict the arc length l_{arc} as it can vary from an arc to another. The arc length depends on atmospheric factors such as temperature and wind.

This method does not take into consideration the phenomenon of the dielectric re-ignition that follows the arc extinction [14].

B. Second Method of Finding G and τ

Another descriptions of G and τ has been suggested in [2]. These are presented in equations (2.26) and (2.27).

$$G = \frac{|i_{arc}|}{V_{arc}} \quad (2.26)$$

$$\tau = Ae^{Bg} \quad (2.27)$$

where i_{arc} is the instantaneous arc current, V_{arc} is the arc voltage constant, and A and B are dimensionless constants. Therefore, this arc model is being customized by the value of three constants V_{arc} , A , and B that shape the behavior of the arc. Also, these three constants vary from an arc to another depending on the system, the fault location, and the atmospheric conditions. To increase the accuracy of the model, it is recommended that these three constants should have two values, one during the positive cycle and another one during the negative cycle.

Unlike the previous method, this model includes the dielectric re-ignition after the arc extinction, but it has been associated with the voltage zero crossings.

2.2 Modeling Petersen Coil System

2.2.1 Background on Earthing System

In three-phase star system e.g. figure 2.8, there is a common connection point called *neutral*. The neutral can be connected to the earth, and in some cases, the neutral point may not be connected to the earth. In addition, the neutral may be connected to a reactor or a resistor with high or low value. These options create different earthing systems that have their advantages or disadvantages depending on the chosen type [18]. Since it is common for MV networks to be star connected, studying the effect of the earthing system becomes important.

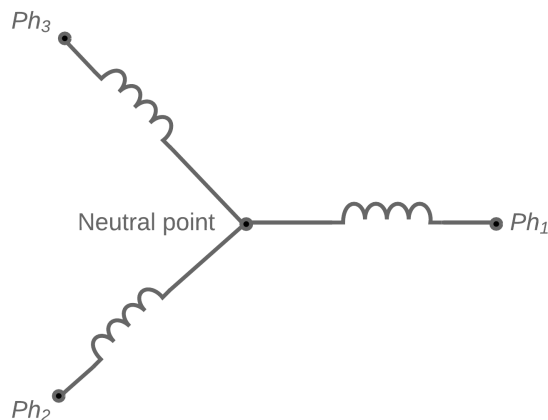


Figure 2.8: Star system with neutral connection [18]

There are three types of neutral connections:

- *Unearthed*: is when the neutral is not connected to the earth.
- *Solidly earthed*: is when the neutral is directly connected to the earth.
- *Impedance-earthed*: is when the neutral is connected to the earth through a resistor or a reactor.

The type of the earthing system can affect the fault voltage and the fault current. An earthed system will have a low fault voltage but a very high fault current. On the other hand, an unearthing system will have a high fault voltage and a low fault current. Determining the type of the earth system depends on the system requirements. The unearthing or high impedance-earthed system will lower the value of the fault current which will allow the system to continue,

but this will not allow the over-current protection system to trip and the system insulation will have to handle the high fault voltage value. An earthed or a low impedance-earthed system will not allow for system continuity since the over-current protection will trip to clear the fault [18].

2.2.2 Petersen Coil System Description

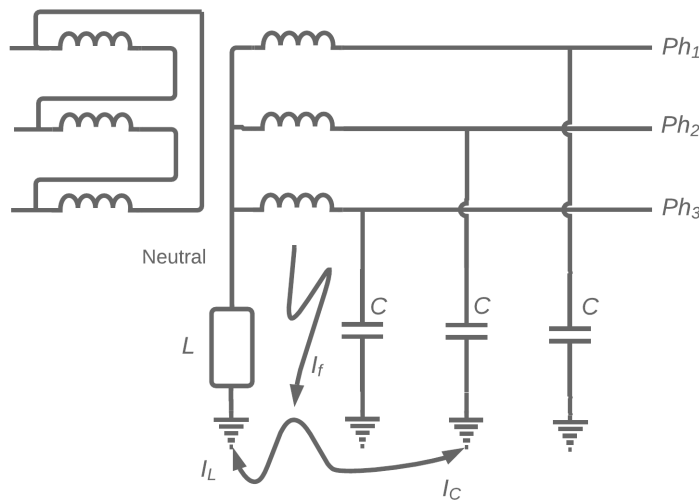


Figure 2.9: Electrical network with a Petersen coil [18]

Figure 2.9 presents a system with a Petersen coil that has a reactor with a value of L that will make the fault current equal to zero. This is as a result of equation (2.28) [18].

$$I_f = I_L + I_{C_1} + I_{C_2} + I_{C_3} \quad (2.28)$$

where I_f is the fault current, I_L is the current in the reactor L , and I_{C_1} , I_{C_2} , and I_{C_3} are the currents in each phase capacitor C .

The current through the reactor can be found using the following equation:

$$I_L = \frac{V_{ph}}{\omega L} \quad (2.29)$$

where V_{ph} is the phase voltage.

Since I_{C_1} , I_{C_2} , and I_{C_3} are equal to each other, the total current through the three phases capacitors I_C can be found using the following equation:

$$I_C = \frac{3V_{ph}}{\frac{1}{\omega C}} = 3V_{ph}\omega C \quad (2.30)$$

Equation (2.28) can be simplified by applying equation (2.29) and (2.30). Also, the size of the reactor L is set to a value that forces the fault current to be equal to zero by having the current I_L is equal to I_C with 180° phase shift.

$$I_L = I_{C_1} + I_{C_2} + I_{C_3} \quad (2.31)$$

$$\frac{V_{ph}}{\omega L} = 3V_{ph}\omega C \quad (2.32)$$

$$L = \frac{1}{3\omega^2 C} \quad (2.33)$$

The reactance of L in the Petersen coil can be tuned to different degrees of the fault compensation as in equation (2.34) [14].

$$L = \frac{1}{3\omega^2 C (1 + \frac{v}{100})} \quad (2.34)$$

where v is the detuning degree in percentage.

2.2.3 Implementing a Parallel Resistor to Petersen Coil Grounding System

In some cases, Petersen coil can be connected with a parallel resistor, which allows some of the active current to pass through it [19]. Figure 2.10 represents this type of connection.

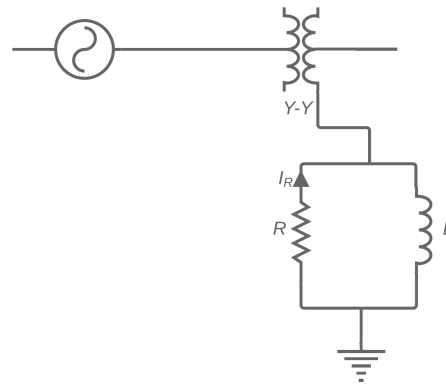


Figure 2.10: Petersen coil with parallel resistor [19]

The resistor R in figure 2.10 can be found using the following equation [19].

$$R = \frac{U_{phase}}{I_R} \quad (2.35)$$

where I_R is the current in resistor R and it can have one of the following standard values: 5, 10, or 15 A.

Chapter 3

Methodology of Modelling the Arc

This chapter will further discuss the implementation of both methods that were presented in section 2.1.2.2 then it will describe the model that was used in the study. The chapter will also present the testing system that is going to be used in verifying the arc model. The same system was also used in studying the effect of varying the detuning level of the Petersen coil and varying the value of the parallel grounding resistor. In addition, the chapter will mention the simulation software that was used in the thesis.

3.1 Simulation Software

Alternative Transients Program of ElectroMagnetic Transients Program (ATP-EMTP) will be used in this thesis a way of implementing and testing the developed arc model [20]. The software enables the users to conduct studies on the electromagnetic phenomena in electric power systems. These studies are conducted with the help of the simulation tools that are inside ATP-EMTP software.

3.2 Arc Models

3.2.1 The Implementation of the First Arc Model

The arc models that is mentioned in [14], has been implemented in ATP-EMTP using a component called *MODEL Type 94* in two different ways.

A. Thevenin Method:

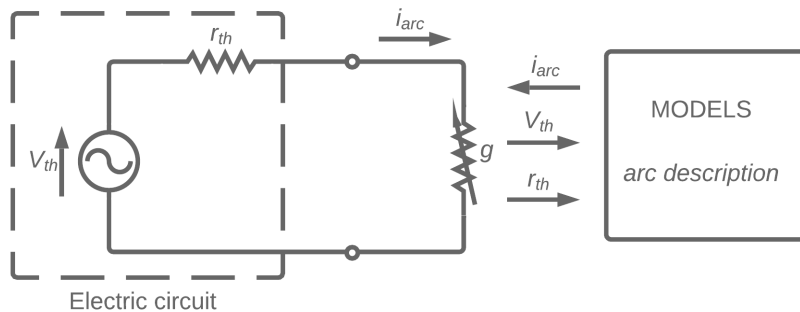


Figure 3.1: The implementation of Thevenin method [14]

Figure 3.1 shows the methodology of implementing the arc model using the Thevenin method. This method takes that value of the Thevenin voltage v_{th} and the Thevenin resistor r_{th} then applies them in equation (3.1) to calculate the arc current i_{arc} .

$$i_{arc} = \frac{g \cdot v_{th}}{1 + g \cdot r_{th}} \quad (3.1)$$

where the arc conductance g can be found by solving equation (2.20) using the Laplace transformation which will lead to the following equation:

$$g(s) = \frac{1}{1 + \tau \cdot s} \cdot G(s) \quad (3.2)$$

In the Thevenin method, MODEL Type 94 component will inject the value of the calculated current into the system after using equation (3.1) and (3.2), which are going to be coded in the component itself.

B. Iterated Method:

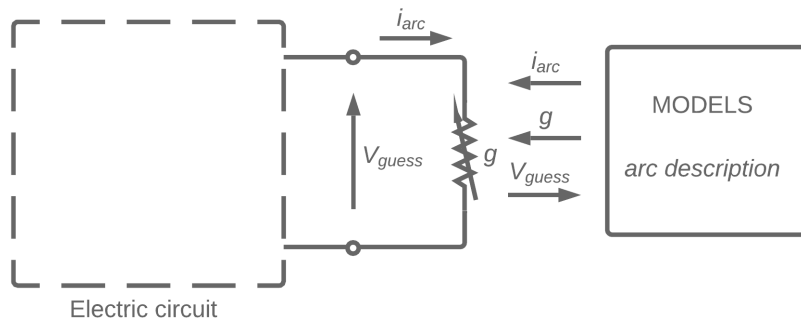


Figure 3.2: The implementation of iterated method [14]

The iterative method is used in ATP-EMTP to calculate the arc voltage and the arc current at each time step by solving the differential equation of the electric circuit and the electric arc. The method is presented in figure 3.2.

$$i_{arc} = g \cdot v_{guess} \quad (3.3)$$

where v_{guess} is the estimated voltage across the arc.

3.2.2 The Implementation of the Second Arc Model

The arc model in [2] has been presented in a block diagram which is in figure 3.3. The model takes the value of the measured arc current along with the preset constants which are V_{arc} , A , and B to find the value of the arc resistance. This resistance value is then being implemented in a varying controlled resistor.

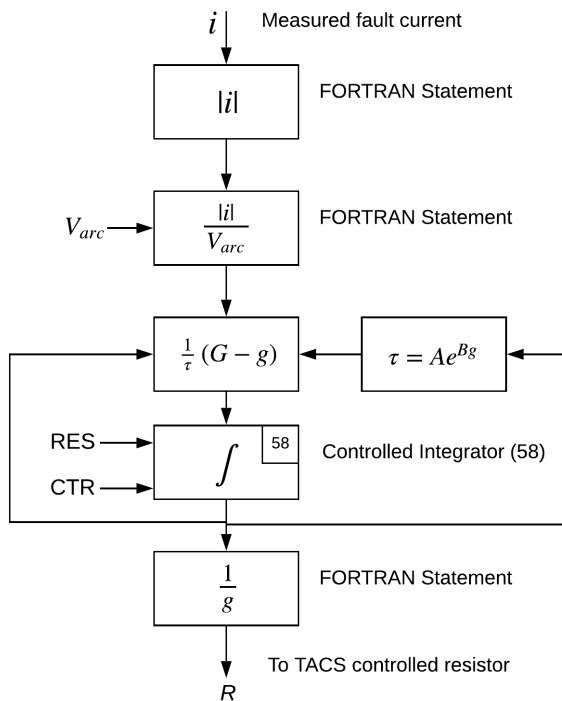


Figure 3.3: The block diagram of the second arc model [2]

The model uses a controlled integrator that passes a reset value RES when the control signal CTR goes to zero. This is to simulate the dielectric re-ignition behavior of the arc. the reset value RES is equal to $0.5 \text{ M}\Omega/\text{ms}$ for a period of 1 ms at the zero-crossing of the voltage sinusoidal waveform, then the value increases to $4 \text{ M}\Omega/\text{ms}$.

3.2.3 Implemented Model in the Study

In this thesis, the equations which are presented in [14] have been implemented using a method that is mentioned in [21]. The diagram of that method can be seen in figure 3.4.

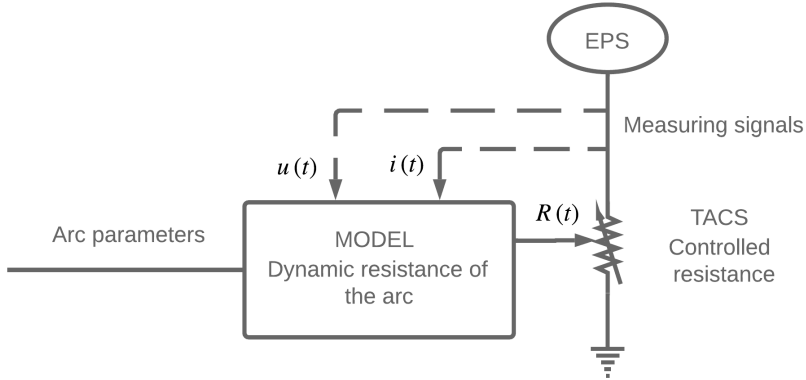


Figure 3.4: Arc fault model with dynamic controlled resistance [21]

The model uses a component in ATP-EMTP software called *MODEL* that takes the value of the fault current and voltage as inputs and send the value of the calculated resistance as an output to a variable controlled resistor. The *MODEL* component can be programmed using FORTRAN language. Figure 3.5 shows the program code which has been used in [21]. This code has been adopted in this thesis and it has been modified, since it does not include some of the arc properties, such as the time-varying arc length and the arc extinction.

```

MODEL Dynamic Arc
INPUT U, Iarc
OUTPUT Rarc, gdyn, Gstat
DATA TAU0 {DFLT:0.25e-3}, Larc {DFLT:0.15}, LO {DFLT:0.15}, alfa {DFLT:-0.4}
VAR gdyn, Gstat, Rarc, U0, R1, TAU
HISTORY gdyn {DFLT:1}
Gstat {DFLT:1}
Rarc {DFLT:1E-8}
INIT
Rarc= 1E-8
ENDINIT
EXEC
TAU:=TAU0* ( (Larc/LO) **alfa)
U0:=(900*Larc)+400
R1:=(0.040*Larc)+0.008
Gstat:=abs(Iarc)/ (U0+(R1*abs(Iarc)))
LAPLACE(gdyn/Gstat):=1.0/(1.0+TAU|s)
Rarc:=recip(gdyn)
ENDEXEC
ENDMODEL

```

Figure 3.5: The dynamic model code [21]

3.3 Testing System

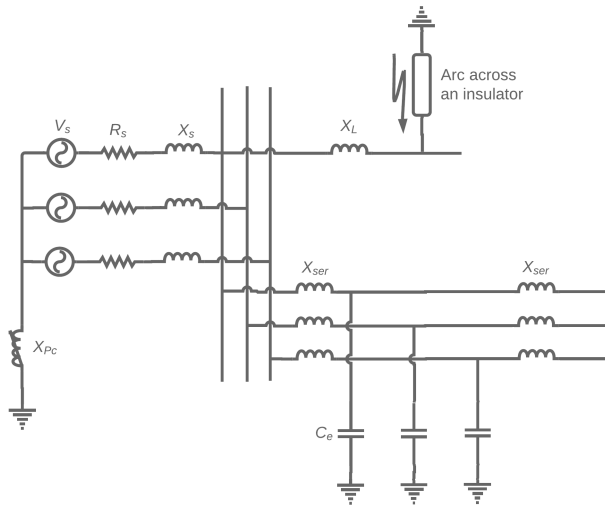


Figure 3.6: Testing system diagram [14]

Figure 3.6 shows the system which was implemented to test the model functionality and to conduct the study. The system has been taken from [14], where it was used in a real and a software simulated tests. The list below is for the system parameters:

- $V_s = 21 \text{ kV}/\sqrt{3}$
- $R_s = 0.096 \Omega$
- $X_s = 1.76 \Omega$
- $X_{ser} = 5 \text{ m}\Omega$
- $X_L = 17.5 \Omega$
- $C_e = 23 \mu\text{F}$

To set the value of Petersen coil X_{Pc} as in [14], equation (2.34) was used for a detuning degree of $v = -20\%$. X_{Pc} was found to be equal to 57.7Ω .

The parameters of the arc model have been stated in [14], and they are:

- $\tau_0 = 0.25 \text{ ms}$
- $\alpha = -0.4$
- $l_0 = 0.20 \text{ m}$

For the time-varying arc length, there are two equations to follow. Equation (3.4) is used when the fault starts at maximum voltage. While Equation (3.5) is used when the fault voltage starts at zero-crossing.

$$\frac{\Delta l}{\Delta t} = \frac{8l_0 - l_0}{200 \text{ ms}} \quad (3.4)$$

$$\frac{\Delta l}{\Delta t} = \frac{8l_0 - l_0}{400 \text{ ms}} \quad (3.5)$$

The arc extinction has been represented using the following limitation:

$$g'_{min} = 50 \mu\text{S} \cdot \text{m}; \frac{dr'}{dt} = 20 \text{ M}\Omega/(\text{s} \cdot \text{m}) \quad (3.6)$$

where g'_{min} is the minimum conductance at which it is assumed that the arc has been self-extinguished, and r' is the arc resistance per unit length [14, 22]. The arc is considered extinguished, if $\frac{dr'}{dt}$ is more than $20 \text{ M}\Omega/(\text{s} \cdot \text{m})$ and g'_{min} is less than $50 \mu\text{S} \cdot \text{m}$. The extinction of the arc has been represented in the model by forcing a large value to the controlled resistor that is equal to $1 \text{ T}\Omega$. In order to avoid having the above limitation affects the model calculations at the fault starting time, a delay of half a period (i.e. 0.01 s) has been implemented in the arc extinction logic.

Since the earth fault is assumed to be crossing the insulator between the over headline conductor and the steel-tower, a resistor with a value of 1Ω has been added to the system.

Chapter 4

Simulation Work and the Study Interests

In this chapter, the system in ATP-EMTP will be presented along with the code for the arc model that has been implemented in the study. The chapter will start by explaining the procedure of implementing the model. Then it will present the study on the effect of changing the detuning factor of Petersen coil. A second study has been conducted on the effect of using different values of a resistor that is parallel to the Petersen grounding coil.

4.1 ATP-EMTP Representation and Arc Model Implementation

The system in figure 3.6 has been implemented in ATP-EMTP as seen in figure 4.1. Two fault scenarios are being considered. The first fault scenario is at voltage maximum and it happens when the switch closes at time $t = 0.02$ s. The second fault scenario occurs when the fault voltage goes at zero and it happens at time $t = 0.025$ s. Figure 4.3 shows the phase voltage of the line without a fault to help in understanding the aforementioned scenarios.

Figure 4.2 shows the programmed code that has been used to simulate the arc fault using the MODEL component. The code uses five variables that have the following meanings:

- tf: is the time starting of the arc fault and it is defined in the ATP-EMTP *Variables* section, as seen in figure 4.5.
- U_MAX: is used to check if the voltage at the maximum of its peak. The sensitivity of U_MAX can be defined in the MODEL screen as it can be seen in figure 4.4.
- U_ZERO: is similar to U_MAX but it is used for checking if the voltage is crossing zero.

- EXTIN: is used to allow the continuation of the arc extinction once it has been achieved.
- L_FUNCTION: is used to segregate the equations of L_{arc} between the two fault scenarios and allow only one function to be used through the whole fault period.

The code uses the derivative function within ATP-EMTP software. It is recommended by [23] to use mid-step derivative instead of the built-in derivative if the time-step does not cover higher frequencies of the signal. The mid-step derivative representation will follow equation (4.1).

$$\frac{\Delta r'}{\Delta t} = \frac{r'_t - r'_{t-1}}{\Delta t} \quad (4.1)$$

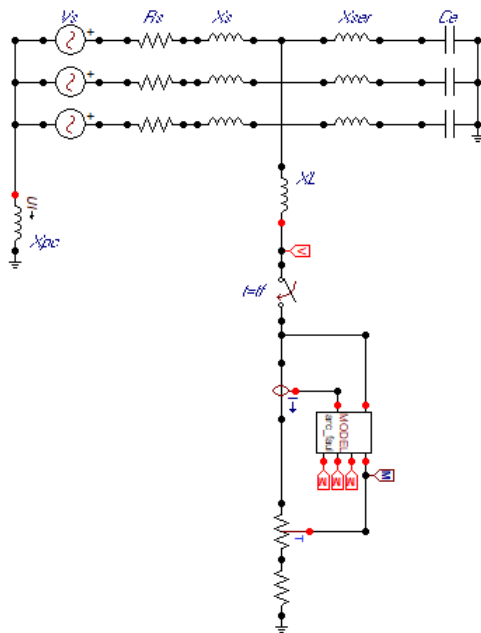


Figure 4.1: System model in ATP-EMTP

```

MODEL Arc_Fault
INPUT U, Iarc
OUTPUT Rarc, Larc, TAU, Ust
DATA TAU0 {DFLT:0.25e-3}, L0 {DFLT:0.2}, alfa {DFLT:-0.4}, tf, U_MAX, U_ZERO
VAR g, Gst, Rarc, Rarcl, U0, R0, TAU, Larc, Ust, EXTIN, L_FUNCTION
HISTORY
g {DFLT:1}
INIT
Larc:= 0.2
EXTIN:= 0
L_FUNCTION:= 0
ENDINIT

EXEC
IF t>=tf AND abs(U)>=U_MAX OR L_FUNCTION=1 THEN
Larc:= Larc+7*L0/200E-3*timestep
L_FUNCTION:= 1
ELSIF t>=tf AND abs(U)<=U_ZERO OR L_FUNCTION=2 THEN
Larc:= Larc+7*L0/400E-3*timestep
L_FUNCTION:= 2
ENDIF

TAU:= TAU0*((Larc/L0)**alfa)
U0:=(900*Larc)+400
R0:=(0.040*Larc)+0.008
Ust:= U0+(R0*abs(Iarc))
Gst:=abs(Iarc)/Ust
LAPLACE(g/Gst):=1.0/(1.0+iTAU/s)
Rarc:=recip(g)

IF g*Larc<50E-6 AND deriv(Rarc)/Larc>20E6 AND t>=tf+0.01 OR EXTIN=1 THEN
Rarc:= 1E12
EXTIN:=1
ELSE
Rarc:=Rarc
ENDIF

ENDEXEC
ENDMODEL

```

Figure 4.2: The arc fault model code

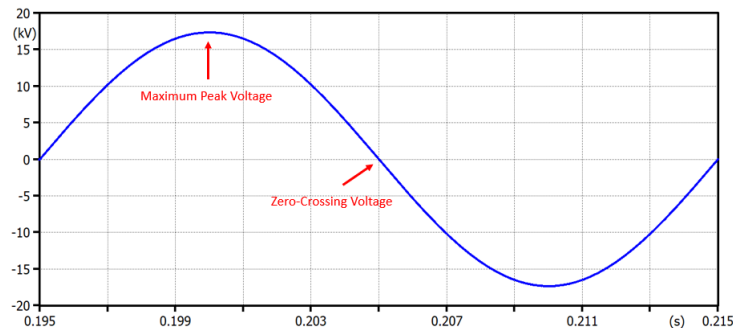


Figure 4.3: Fault scenarios

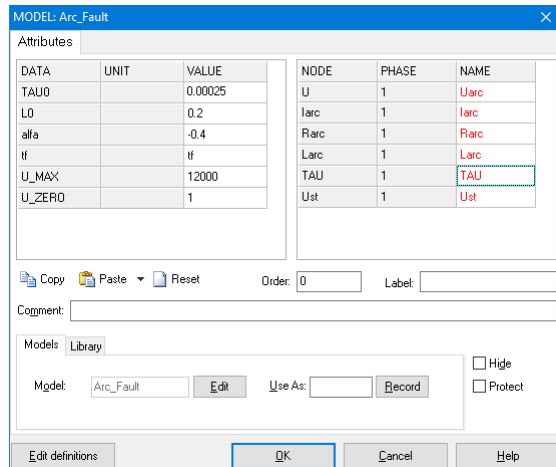


Figure 4.4: MODEL component in ATP-EMTP

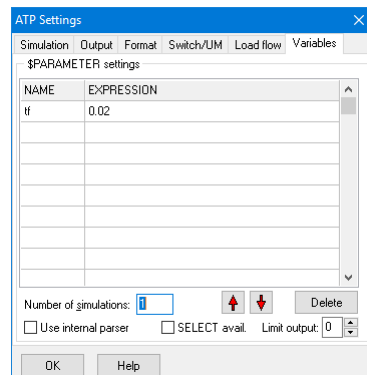


Figure 4.5: Implemented fault time in ATP-EMTP

4.2 Studying the Effect of Petersen Coil

To study the effect of Petersen coil, the value of X_{Pc} has been detuned at different levels, while assuming that the arc characteristics will be the same as the original system across all detuning levels. Table 4.1 shows the calculated X_{Pc} values by using equation (2.34). The effect of each level has been tested when the fault happens at the voltage maximum and zero.

Table 4.1: The studied Petersen coil detuning levels

Detuning Degree v	X_{Pc} (Ω)
-20%	57.7
-15%	54.3
-10%	51.3
-5%	48.6
0%	46.1
+5%	43.9
+10%	41.9
+15%	40.1
+20%	38.4

4.3 Studying the Effect of Petersen Coil Parallel Resistor

In this part of the study, the resistor R_{Pc} in figure 4.6 has been added to be in parallel with grounding inductor X_{Pc} . The value of R_{Pc} was calculated using equation (2.35) and by implementing the typical values of active current I_R that are mentioned in section 2.2.3. The result of these calculations can be seen in table 4.2.

Table 4.2: Values of Petersen coil parallel resistor used in the study

I_R (A)	R_{Pc} ($k\Omega$)
5	2.4249
10	1.2124
15	0.8083

The tests were made with a varies value of the Petersen coil X_{Pc} that was tuned from $v = -20\%$ to $v = +20\%$. This will allow studying the effect of implementing a parallel resistor to the original system at different detuning levels. In addition, it is assumed that the arc characteristics will be the same

in all detuning levels as the original system. These characteristics have been previously mentioned in section 3.3.

Similar to section 4.2, the effect of the parallel resistor will be studied when the fault starts at the voltage maximum and voltage zero-crossing.

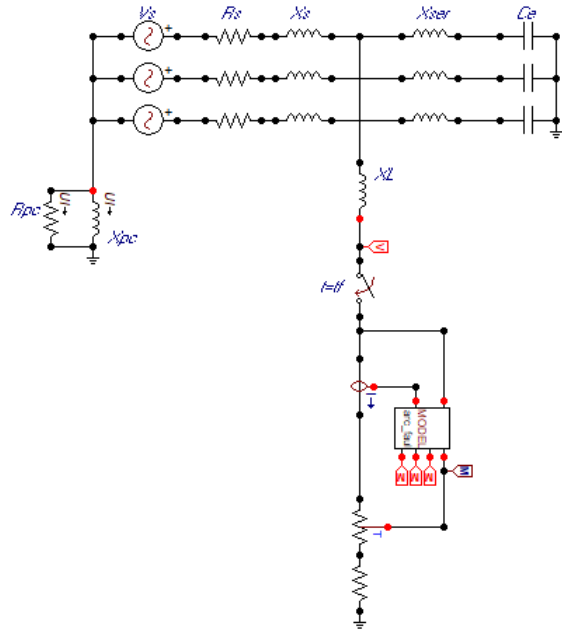


Figure 4.6: System model with a parallel grounding resistor

Chapter 5

Simulation Results

The chapter will present the results that were obtained from the study. It will start with the original system that was used for testing and confirming the arc model response. Then it will be followed by the other results from studying the effect of varying the value of the Petersen coil and varying the value of the parallel grounding resistor.

5.1 Initial Arc Model Implementation Results

This section will show the simulated results against the expected results from [14], which will help in comparing the differences and confirming the model functionality. The section will also present the behavior of the arc length, arc resistance, stationary arc voltage, and arc time constant during the fault. As been stated in section 4.1, two scenarios are being tested. The first scenario is when the fault occurs at the maximum peak voltage. The second scenario is when the voltage crosses the zero.

5.1.1 Fault Inception at Voltage Maximum

Figures 5.1, 5.2, and 5.3 are the arc voltage, arc current, and the Petersen coil arc current, respectively. These three figures present simulated results versus the expected results from [14] for the scenario when the test was conducted at the system's voltage maximum. Figure 5.4 shows the arc length that was calculated using equation (3.4). Figures 5.5, 5.6, and 5.7 are the output arc resistance, stationary arc voltage, and the arc length, respectively.

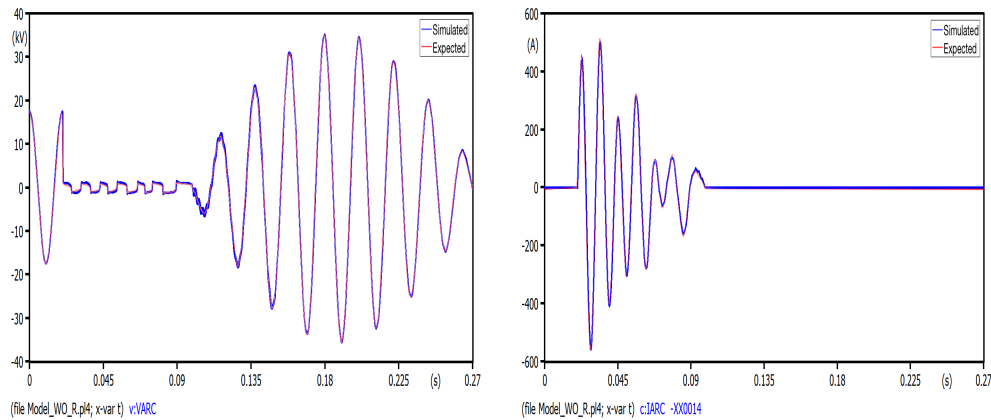


Figure 5.1: Simulated vs expected fault voltage when fault inception at voltage maximum

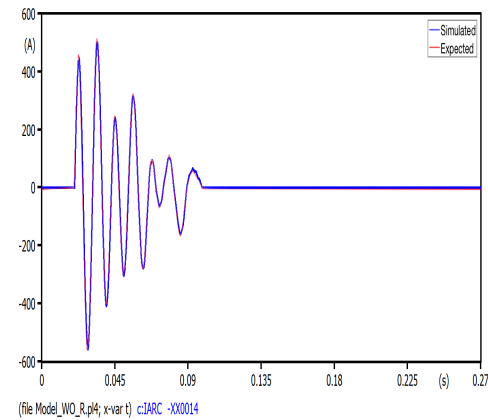


Figure 5.2: Simulated vs expected fault current when fault inception at voltage maximum

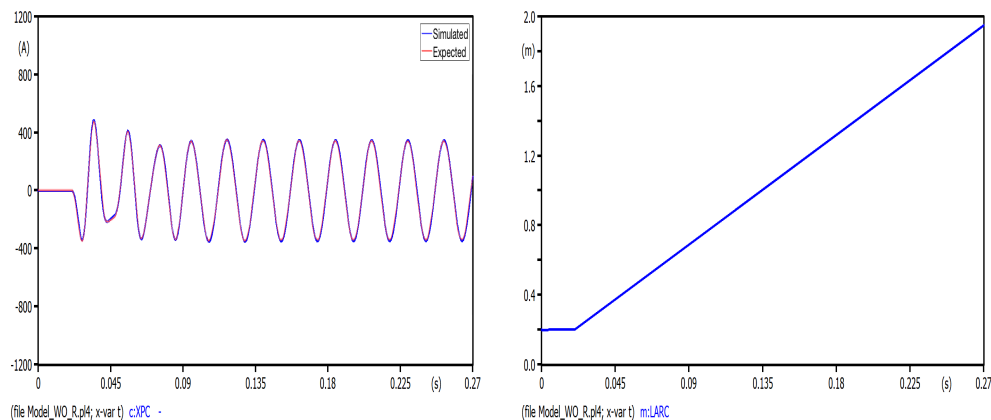


Figure 5.3: Simulated vs expected Petersen coil current when fault inception at voltage maximum

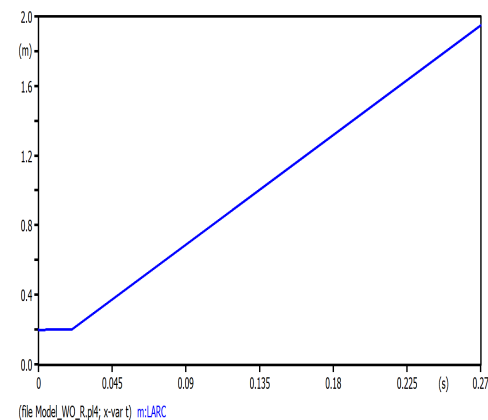


Figure 5.4: Simulated arc length when fault inception at voltage maximum

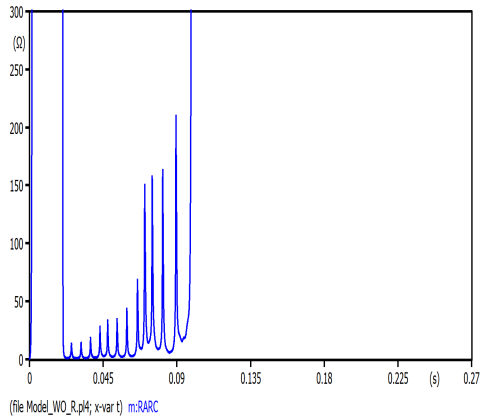


Figure 5.5: Simulated arc resistance when fault inception at voltage maximum

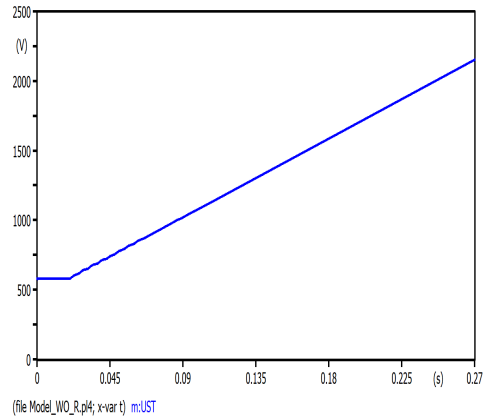


Figure 5.6: Simulated stationary arc voltage when fault inception at voltage maximum

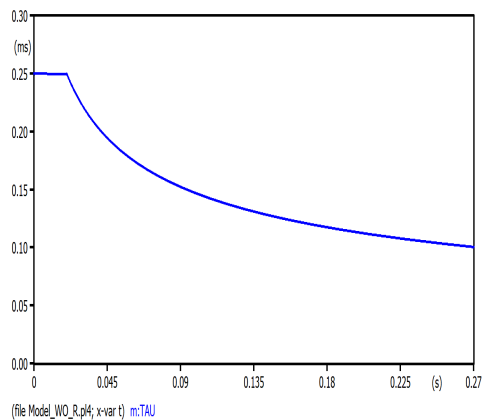


Figure 5.7: Simulated arc time constant when fault inception at voltage maximum

5.1.2 Fault Inception at Voltage Zero-Crossing

This section shows the system functional test of the second scenario where the fault starts when the voltage is crossing zero. Figures 5.8, 5.9, and 5.10 present the expected versus the simulated arc voltage, arc current, and Petersen coil arc current, respectively. Figure 5.11 illustrates the calculated arc length using equation (3.4), while figures 5.12, 5.13, and 5.14 reveal the simulated arc resistance, stationary arc voltage, and arc time constant, respectively.

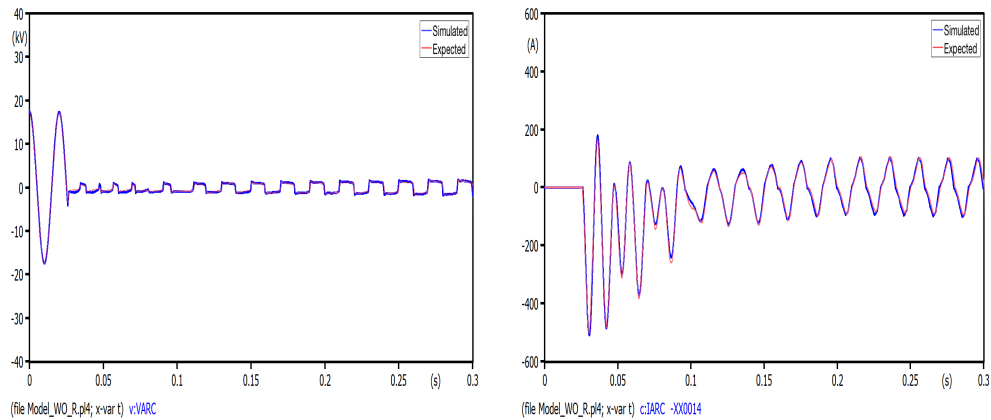


Figure 5.8: Simulated vs expected fault voltage when fault inception at voltage zero-crossing

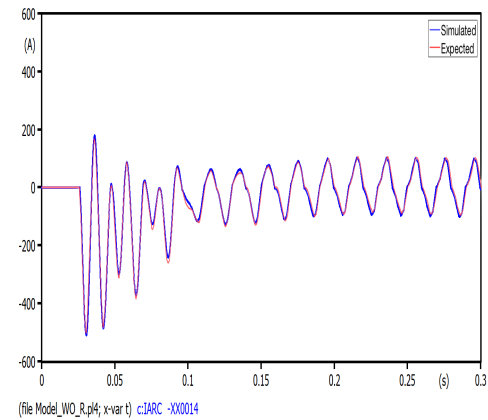


Figure 5.9: Simulated vs expected fault current when fault inception at voltage zero-crossing

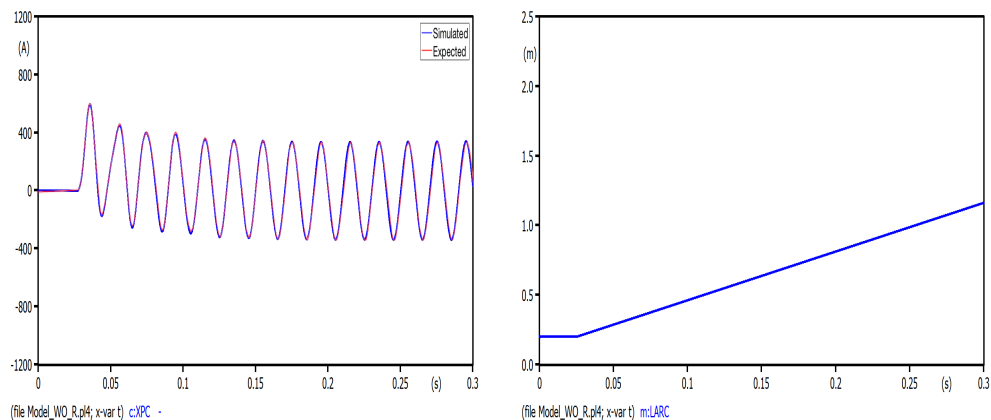


Figure 5.10: Simulated vs expected Petersen coil current when fault inception at voltage zero-crossing

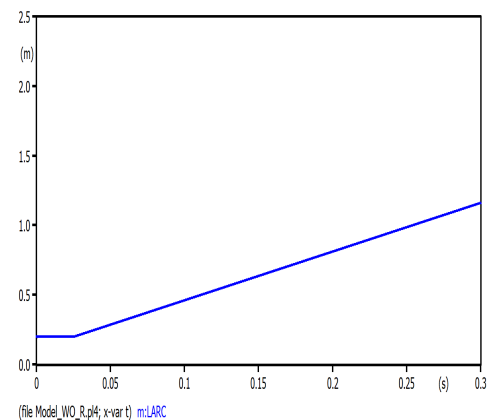


Figure 5.11: Simulated arc length when fault inception at voltage zero-crossing

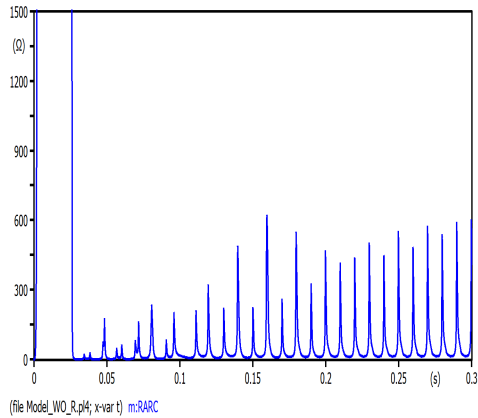


Figure 5.12: Simulated arc resistance when fault inception at voltage zero-crossing

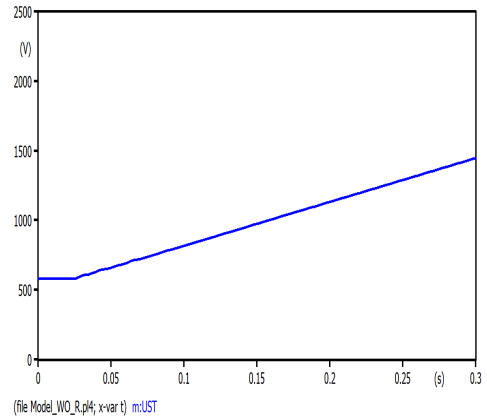


Figure 5.13: Simulated stationary arc voltage when fault inception at voltage zero-crossing

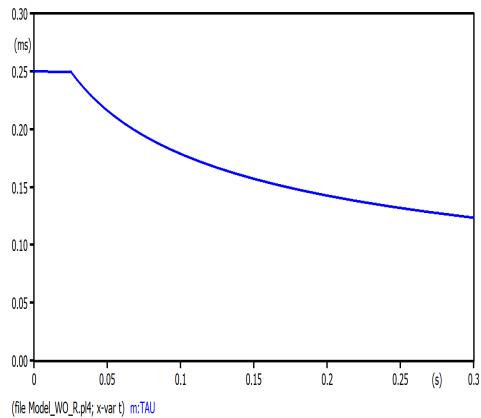


Figure 5.14: Simulated arc time constant when fault inception at voltage zero-crossing

5.2 Results from Detuning Petersen Coil at Different Degrees

In this section, the results from changing the detuning degree v of the Petersen coil will be studied. Table 4.1 shows the values that are going to be used in the study. Each of the detuning degrees will be presented in a subsection, where each subsection will provide the resulted arc voltage and current. This study has also included the effect of fault inception location, whether at voltage maximum or zero-crossing.

5.2.1 Fault Inception at Voltage Maximum

5.2.1.1 Arc Voltage Measurements

Figures 5.15 - 5.23 show the results of the arc voltage that was measured by the simulation while detuning the Petersen coil between -20% to $+20\%$ and when the fault started at the maximum peak of the line voltage.

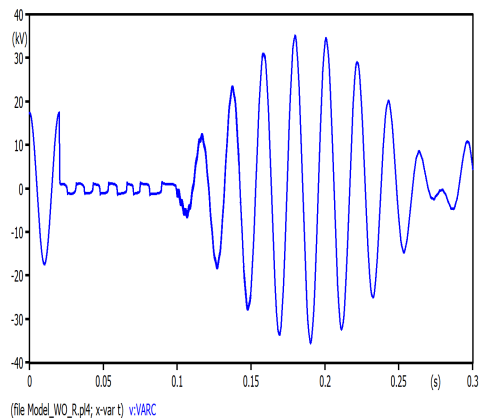


Figure 5.15: Fault voltage when detuning degree at -20% and fault inception at voltage maximum

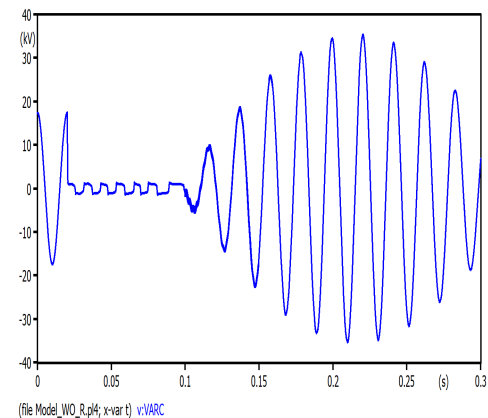


Figure 5.16: Fault voltage when detuning degree at -15% and fault inception at voltage maximum

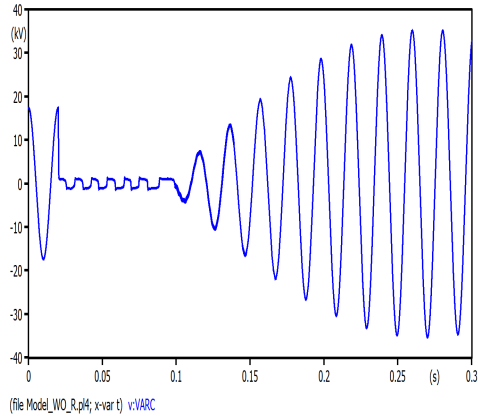


Figure 5.17: Fault voltage when detuning degree at -10% and fault inception at voltage maximum

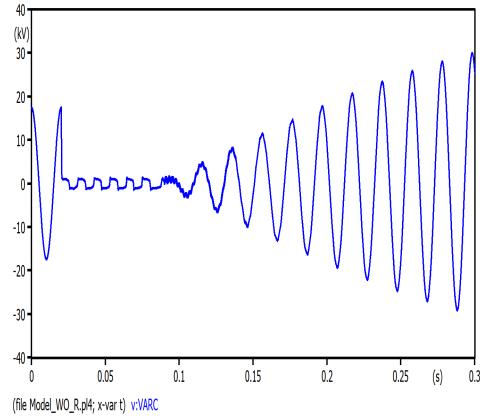


Figure 5.18: Fault voltage when detuning degree at -5% and fault inception at voltage maximum

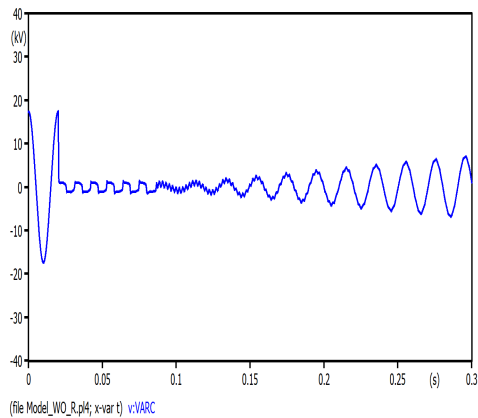


Figure 5.19: Fault voltage when detuning degree at 0% and fault inception at voltage maximum

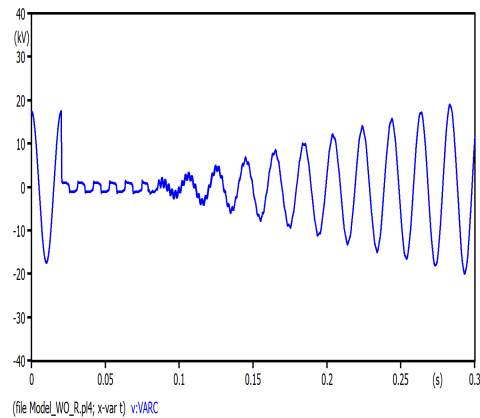


Figure 5.20: Fault voltage when detuning degree at +5% and fault inception at voltage maximum

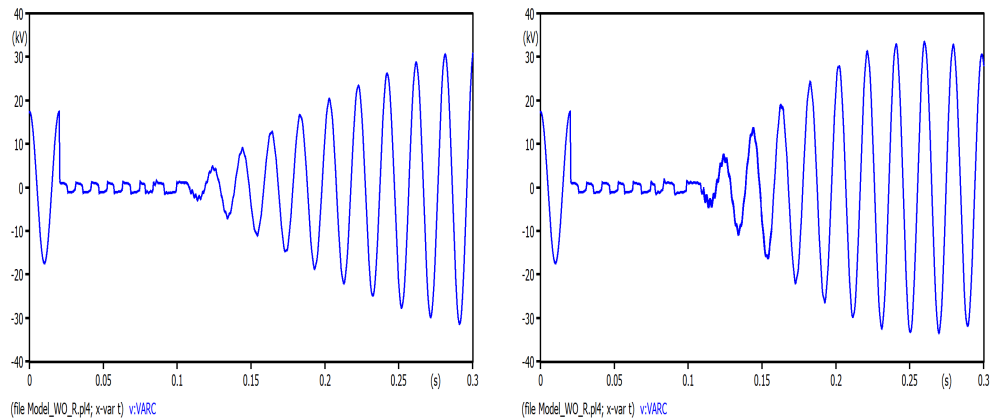


Figure 5.21: Fault voltage when detuning degree at +10% and fault inception at voltage maximum

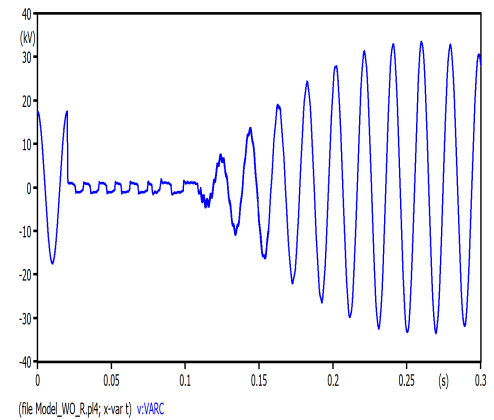


Figure 5.22: Fault voltage when detuning degree at +15% and fault inception at voltage maximum

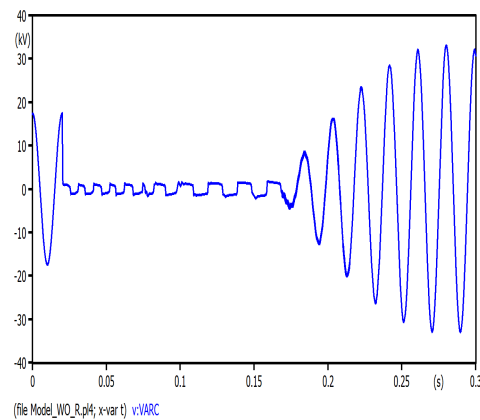


Figure 5.23: Fault voltage when detuning degree at +20% and fault inception at voltage maximum

5.2.1.2 Arc Current Measurements

Similar to section 5.2.1.1, figures 5.24 - 5.32 present the results of the arc current that was measured while applying the simulation under the same conditions.

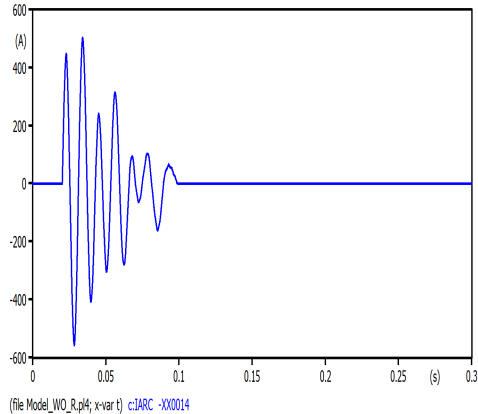


Figure 5.24: Fault current when detuning degree at -20% and fault inception at voltage maximum

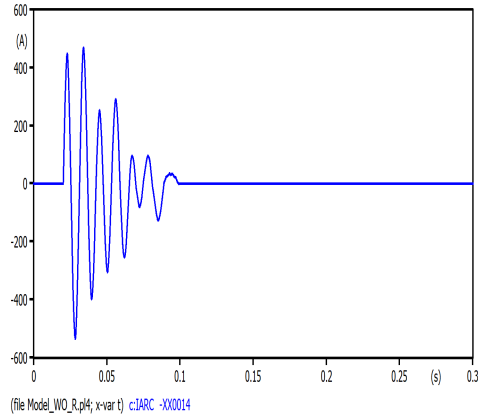


Figure 5.25: Fault current when detuning degree at -15% and fault inception at voltage maximum

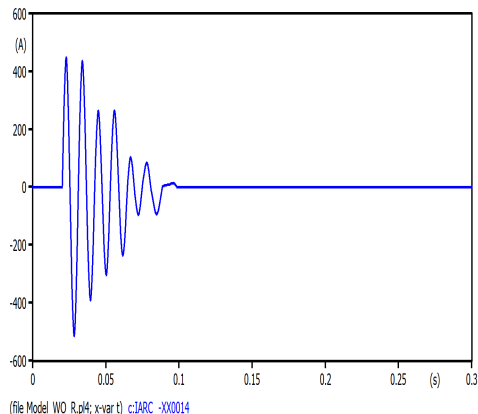


Figure 5.26: Fault current when detuning degree at -10% and fault inception at voltage maximum

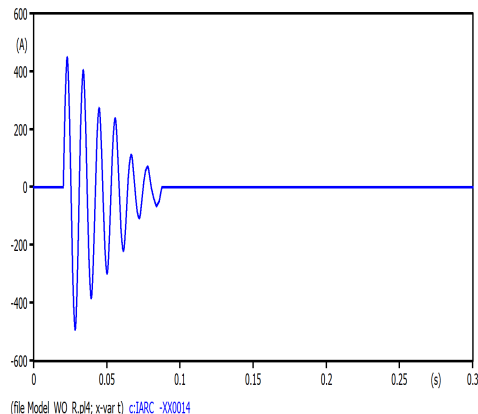


Figure 5.27: Fault current when detuning degree at -5% and fault inception at voltage maximum

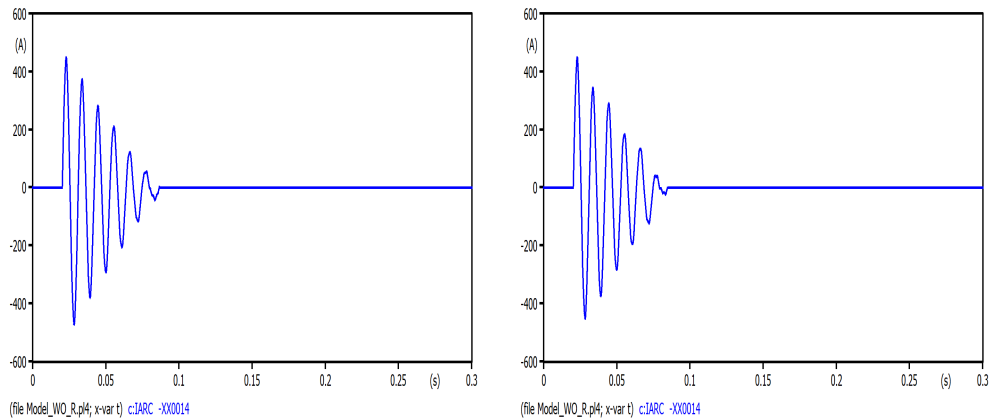


Figure 5.28: Fault current when detuning degree at 0% and fault inception at voltage maximum

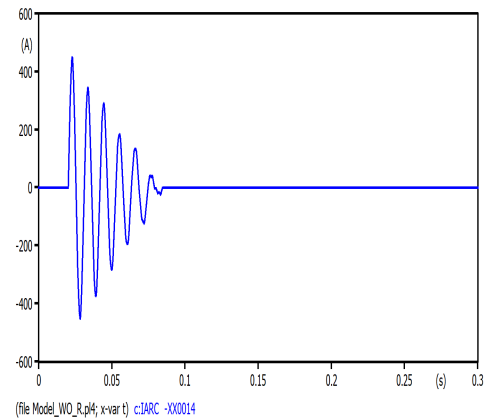


Figure 5.29: Fault current when detuning degree at +5% and fault inception at voltage maximum

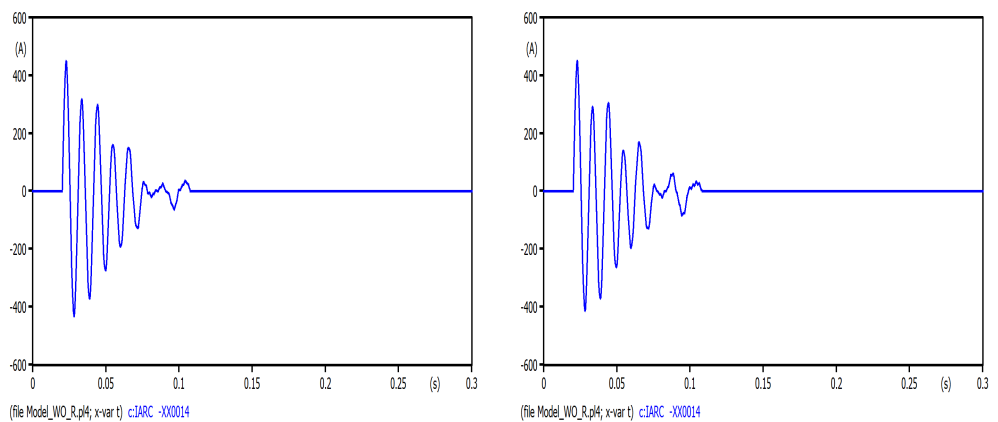


Figure 5.30: Fault current when detuning degree at +10% and fault inception at voltage maximum

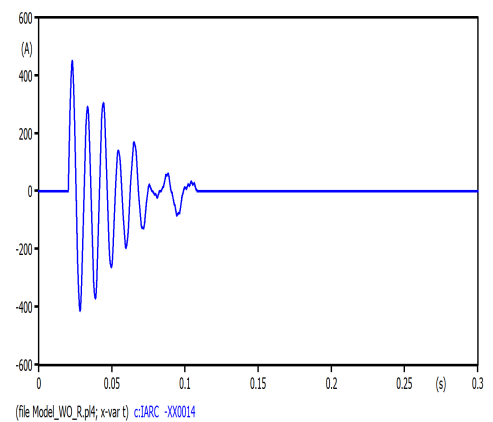


Figure 5.31: Fault current when detuning degree at +15% and fault inception at voltage maximum

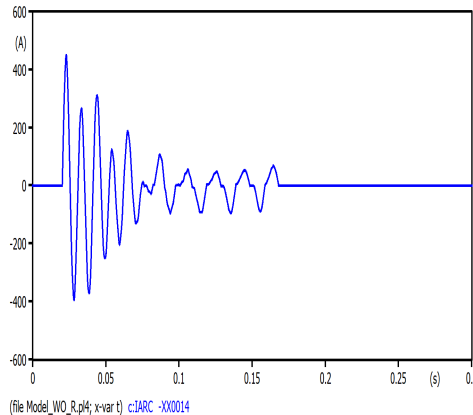


Figure 5.32: Fault current when detuning degree at +20% and fault inception at voltage maximum

5.2.2 Fault Inception at Voltage Crossing Zero

5.2.2.1 Arc Voltage Measurements

Figures 5.33 - 5.41 show the results of the arc voltage that was measured by the simulation while detuning the Petersen coil between -20% to $+20\%$ and when the fault started at the point at which the line voltage is crossing zero.

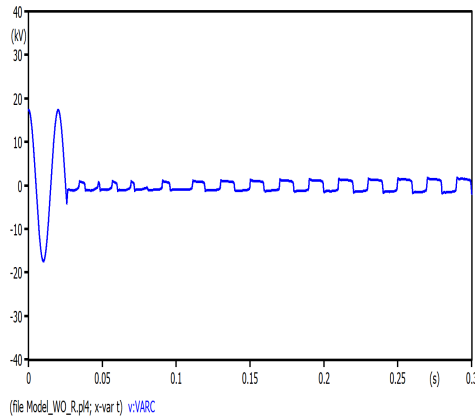


Figure 5.33: Fault voltage when detuning degree at -20% and fault inception at voltage zero-crossing

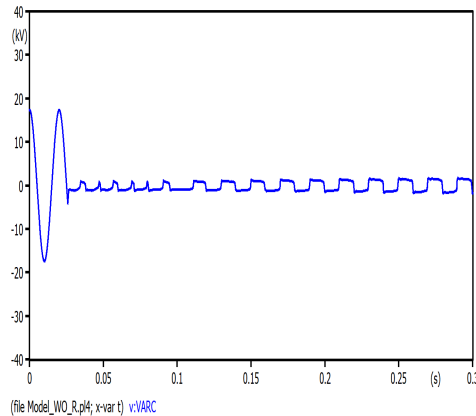


Figure 5.34: Fault voltage when detuning degree at -15% and fault inception at voltage zero-crossing

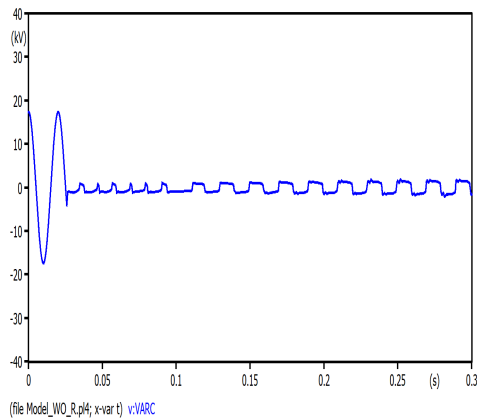


Figure 5.35: Fault voltage when detuning degree at -10% and fault inception at voltage zero-crossing

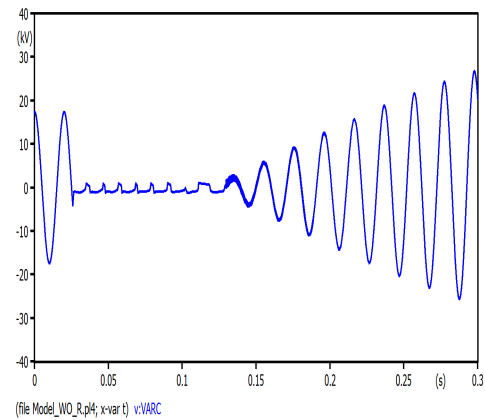


Figure 5.36: Fault voltage when detuning degree at -5% and fault inception at voltage zero-crossing

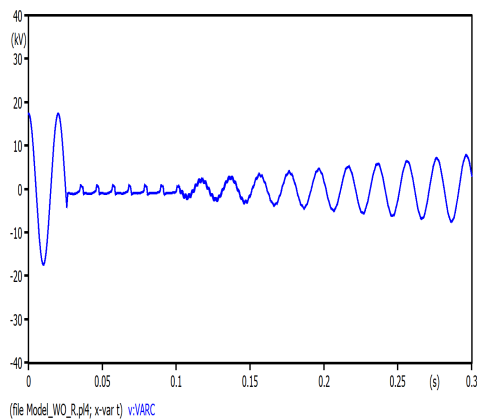


Figure 5.37: Fault voltage when detuning degree at 0% and fault inception at voltage zero-crossing

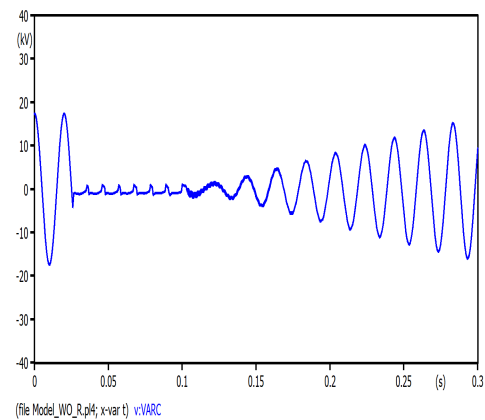


Figure 5.38: Fault voltage when detuning degree at +5% and fault inception at voltage zero-crossing

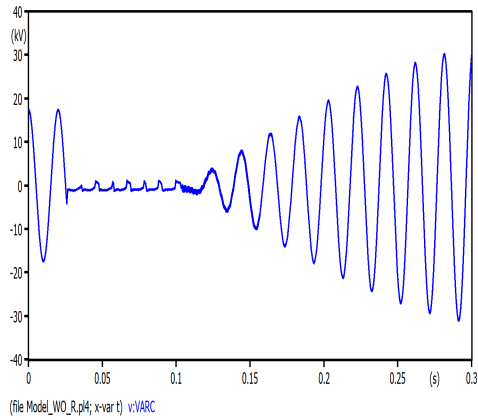


Figure 5.39: Fault voltage when detuning degree at +10% and fault inception at voltage zero-crossing

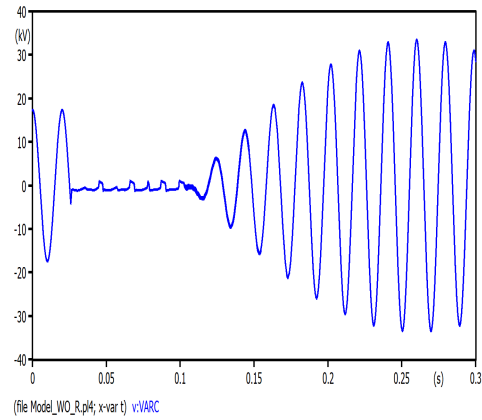


Figure 5.40: Fault voltage when detuning degree at +15% and fault inception at voltage zero-crossing

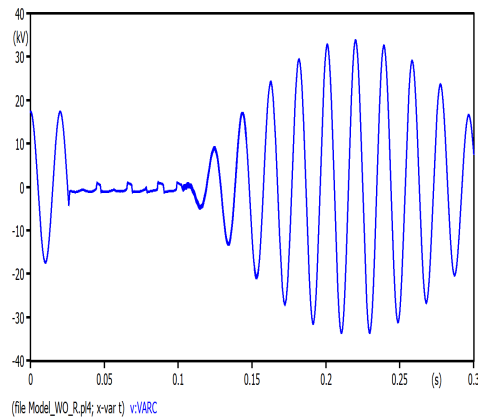


Figure 5.41: Fault voltage when detuning degree at +20% and fault inception at voltage zero-crossing

5.2.2.2 Arc Current Measurements

As been discussed in section 5.2.2.1, figures 5.42 - 5.50 illustrate the results of the arc current that was measured while applying the simulation under the same conditions.

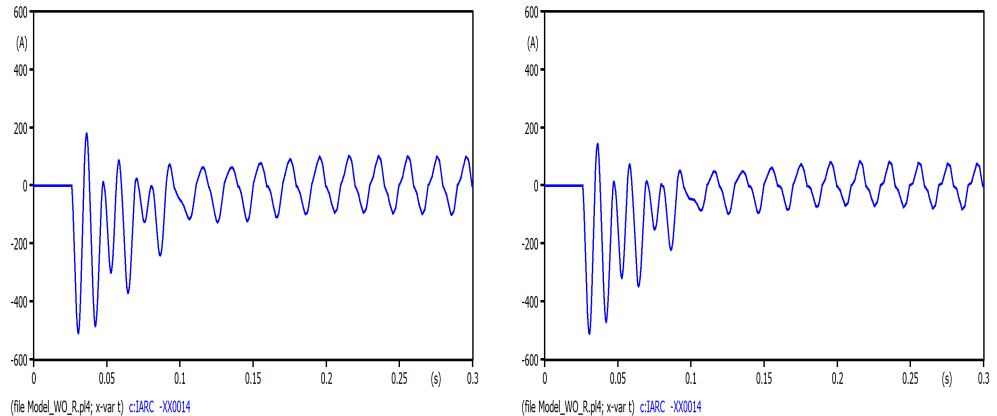


Figure 5.42: Fault current when detuning degree at -20% and fault inception at voltage zero-crossing

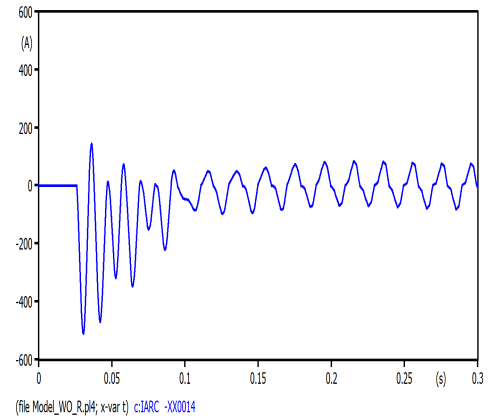


Figure 5.43: Fault current when detuning degree at -15% and fault inception at voltage zero-crossing

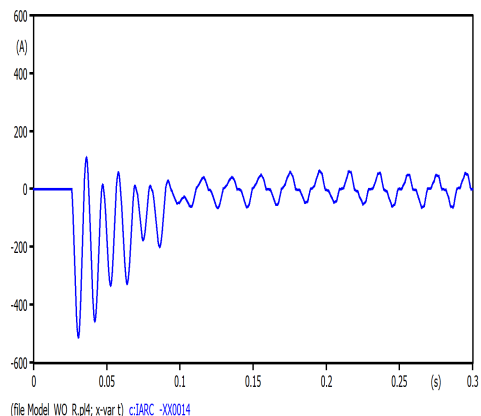


Figure 5.44: Fault current when detuning degree at -10% and fault inception at voltage zero-crossing

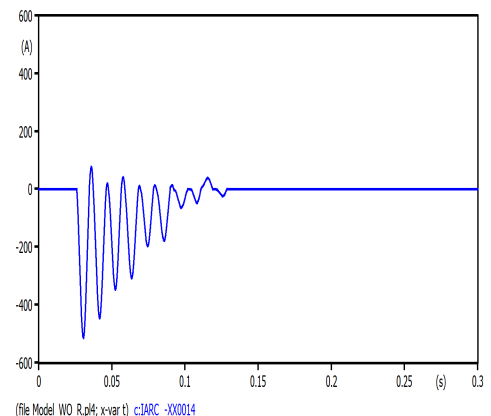


Figure 5.45: Fault current when detuning degree at -5% and fault inception at voltage zero-crossing

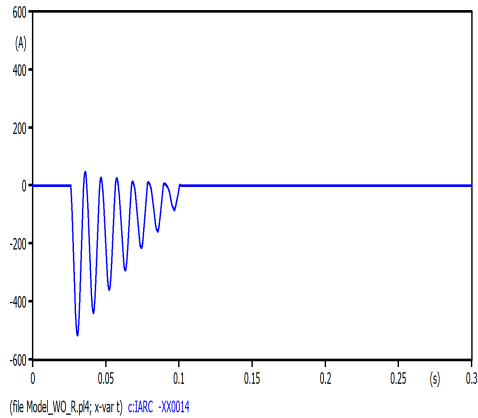


Figure 5.46: Fault current when detuning degree at 0% and fault inception at voltage zero-crossing

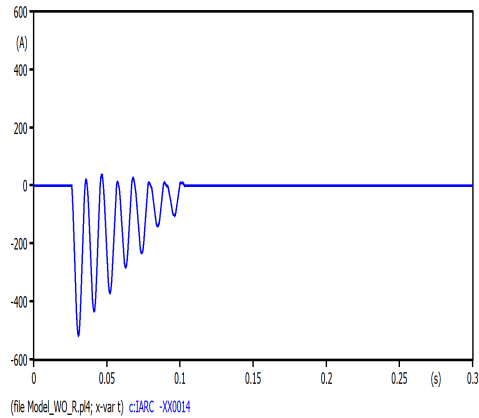


Figure 5.47: Fault current when detuning degree at +5% and fault inception at voltage zero-crossing

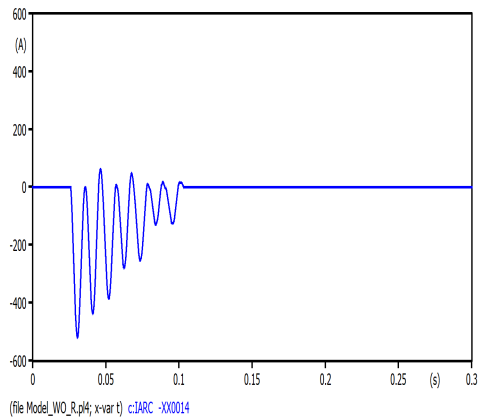


Figure 5.48: Fault current when detuning degree at +10% and fault inception at voltage zero-crossing

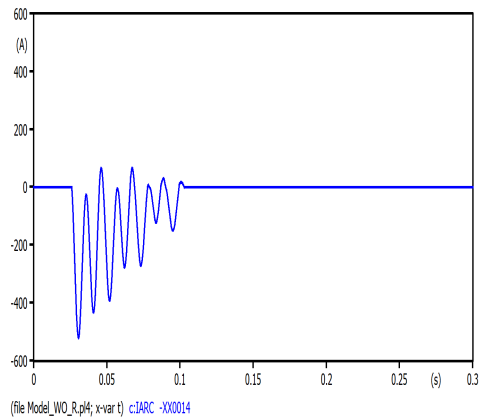


Figure 5.49: Fault current when detuning degree at +15% and fault inception at voltage zero-crossing

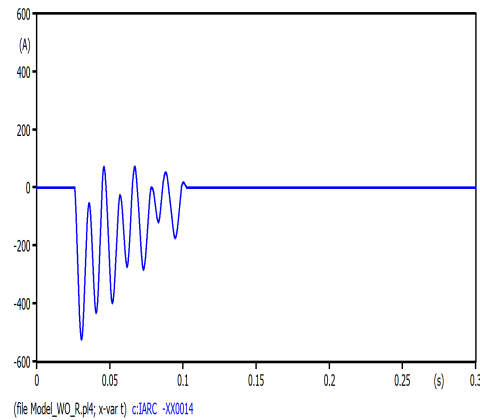


Figure 5.50: Fault current when de-tuning degree at +20% and fault inception at voltage zero-crossing

5.3 Results When Adding a Parallel Ground Resistor

Similar to section 5.2, the system will be tested with the same fault scenarios but with having a resistor that is in parallel to the Petersen coil.

5.3.1 Fault Inception at Voltage Maximum

5.3.1.1 Arc Voltage Measurements

Figures 5.51 - 5.59 show the results of the arc voltages from detuning the resonance coils between -20% to $+20\%$ while the fault occurs at the peak of the line voltage. Each figure presents the resulted arc voltage when implementing all the values of the parallel grounding resistor that are mentioned in table 4.2.

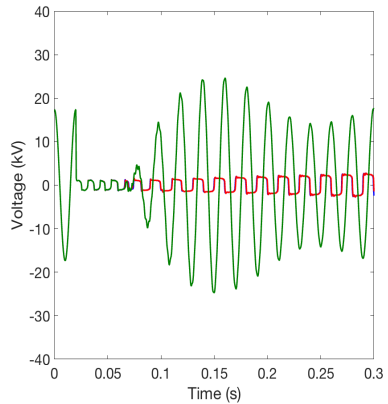


Figure 5.51: Fault voltages when de-tuning degree at -20% and fault inception at voltage maximum

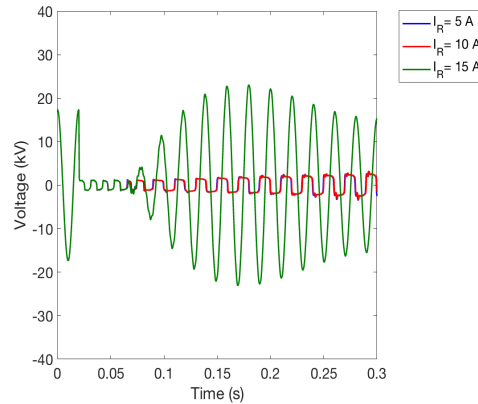


Figure 5.52: Fault voltages when de-tuning degree at -15% and fault inception at voltage maximum

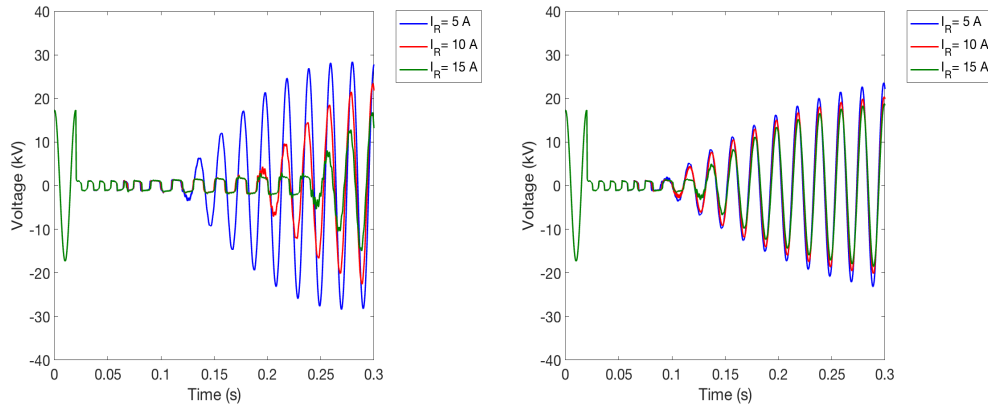


Figure 5.53: Fault voltages when detuning degree at -10% and fault inception at voltage maximum

Figure 5.54: Fault voltages when detuning degree at -5% and fault inception at voltage maximum

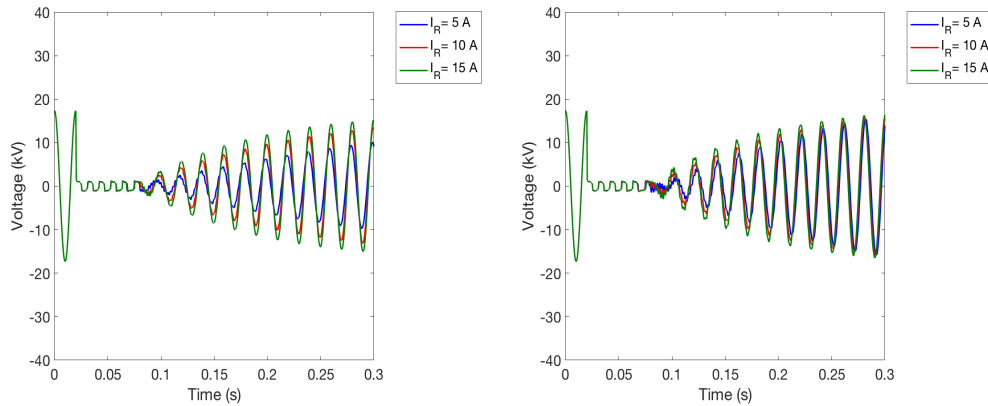


Figure 5.55: Fault voltages when detuning degree at 0% and fault inception at voltage maximum

Figure 5.56: Fault voltages when detuning degree at +5% and fault inception at voltage maximum

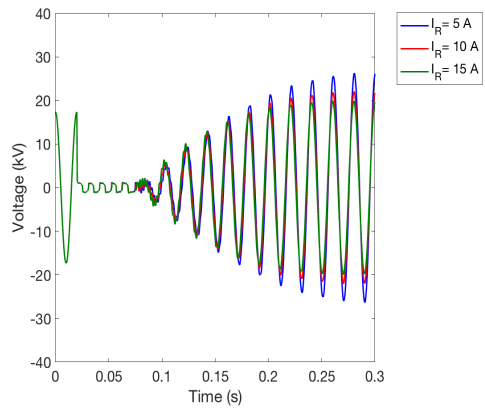


Figure 5.57: Fault voltages when detuning degree at +10% and fault inception at voltage maximum

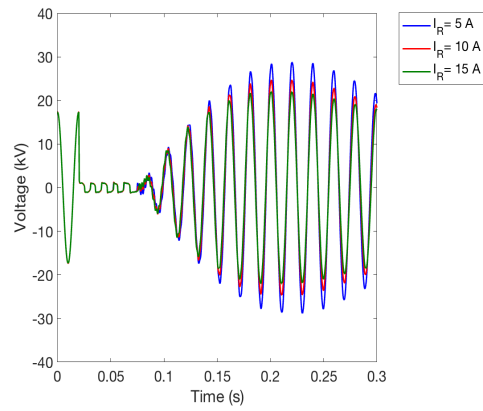


Figure 5.58: Fault voltages when detuning degree at +15% and fault inception at voltage maximum

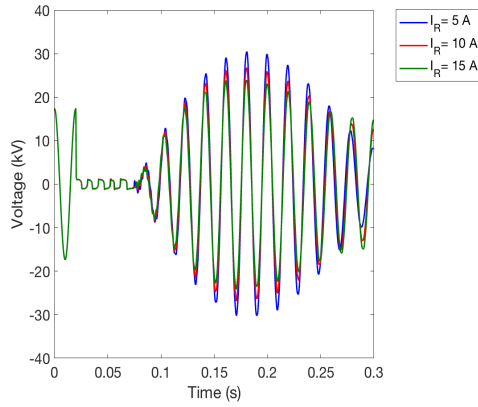


Figure 5.59: Fault voltages when detuning degree at +20% and fault inception at voltage maximum

5.3.1.2 Arc Current Measurements

Following section 5.3.1.1, figures 5.60 - 5.68 illustrate the resulted arc currents while applying the same testing conditions.

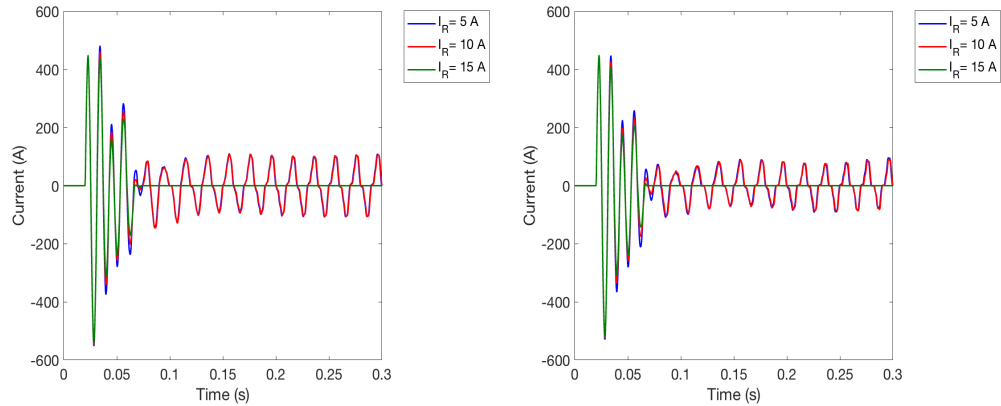


Figure 5.60: Fault currents when detuning degree at -20% and fault inception at voltage maximum

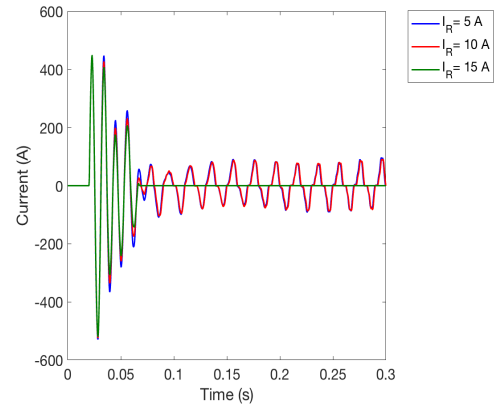
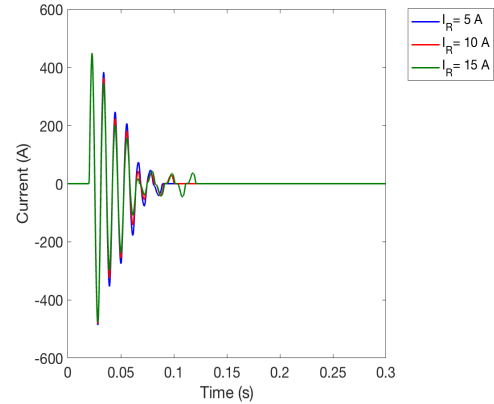
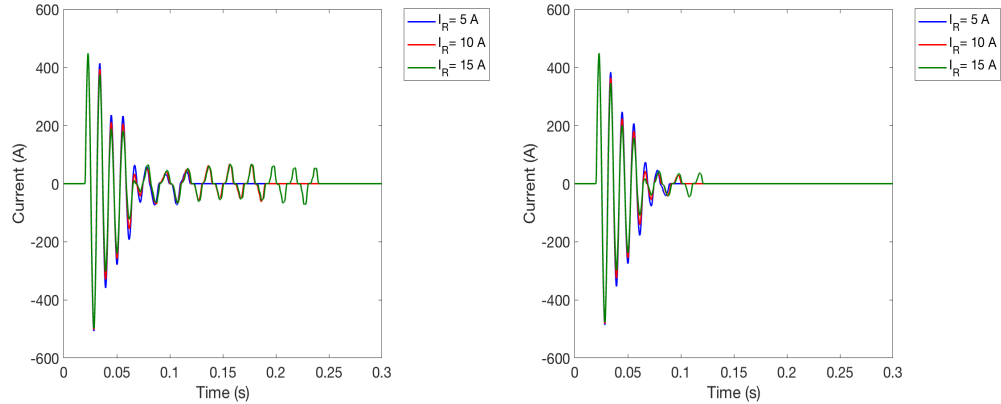


Figure 5.61: Fault currents when detuning degree at -15% and fault inception at voltage maximum



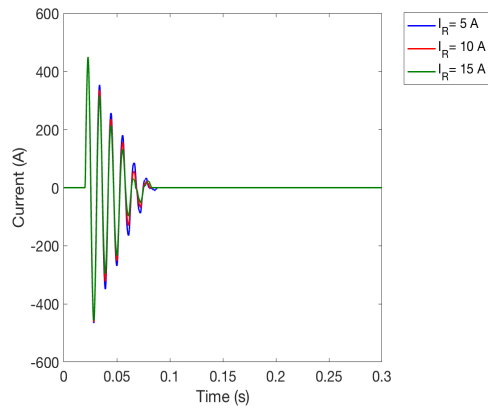


Figure 5.64: Fault currents when detuning degree at 0% and fault inception at voltage maximum

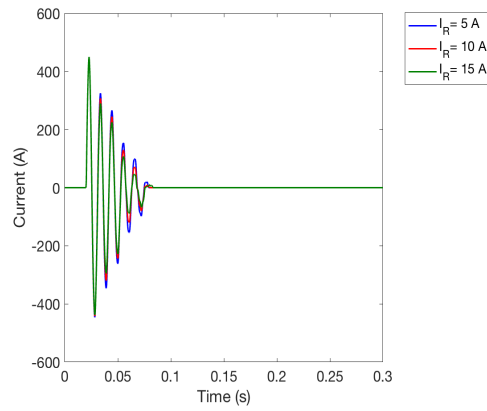


Figure 5.65: Fault currents when detuning degree at +5% and fault inception at voltage maximum

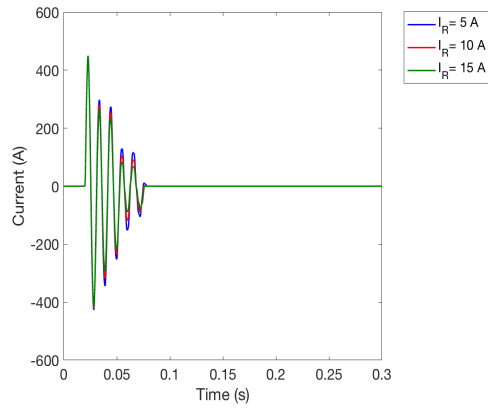


Figure 5.66: Fault currents when detuning degree at +10% and fault inception at voltage maximum

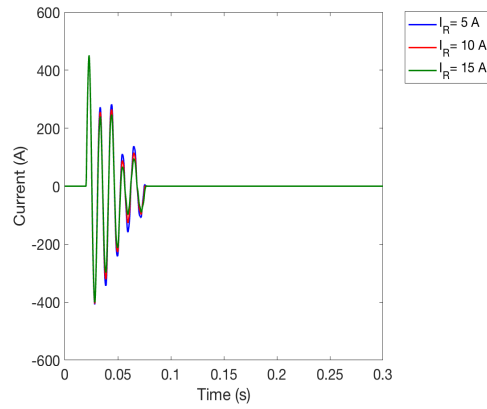


Figure 5.67: Fault currents when detuning degree at +15% and fault inception at voltage maximum

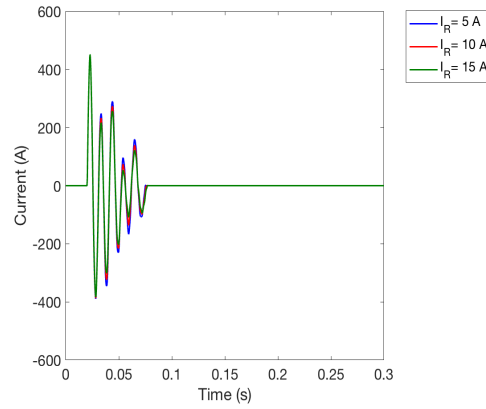


Figure 5.68: Fault currents when detuning degree at +20% and fault inception at voltage maximum

5.3.2 Fault Inception at Voltage Crossing Zero

5.3.2.1 Arc Voltage Measurements

Figures 5.69 - 5.77 present the results of the arc voltages from detuning the resonance coils between -20% to $+20\%$ while the fault occurs at the zero-crossing point of the line voltage. Similar to section 5.3.1.1, each figure shows the results of implementing all the values of the parallel grounding resistor that are in table 4.2.

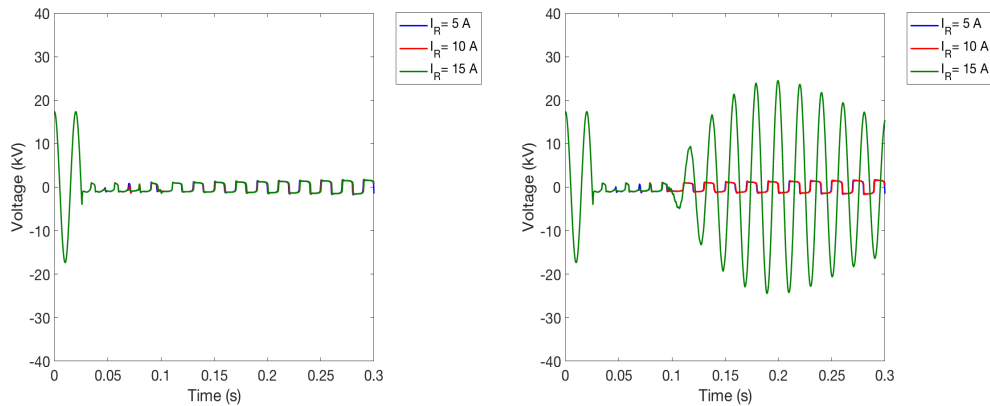


Figure 5.69: Fault voltages when detuning degree at -20% and fault inception at voltage zero-crossing

Figure 5.70: Fault voltages when detuning degree at -15% and fault inception at voltage zero-crossing

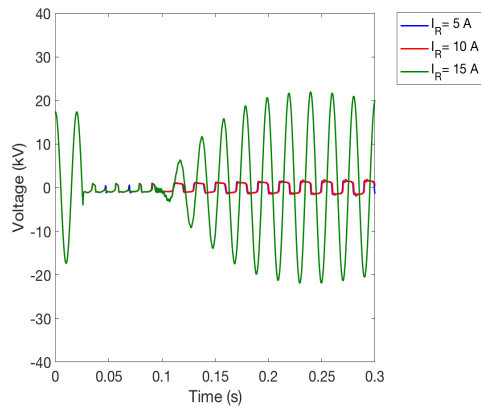


Figure 5.71: Fault voltages when detuning degree at -10% and fault inception at voltage zero-crossing

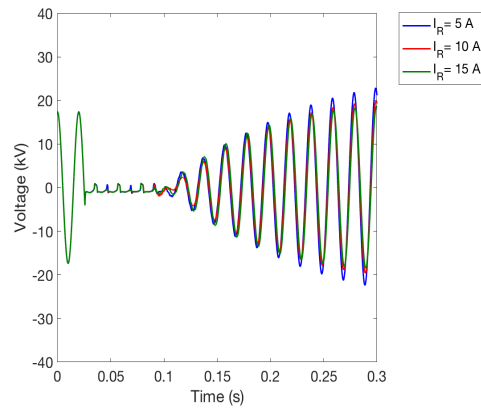


Figure 5.72: Fault voltages when detuning degree at -5% and fault inception at voltage zero-crossing

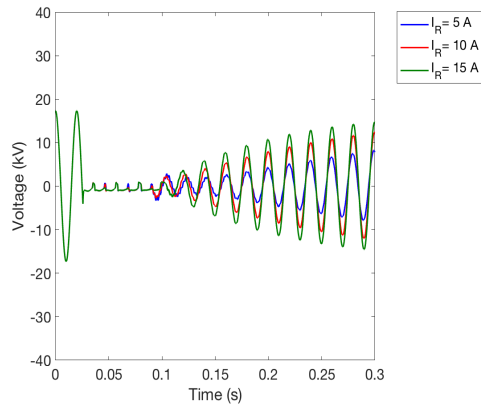


Figure 5.73: Fault voltages when detuning degree at 0% and fault inception at voltage zero-crossing

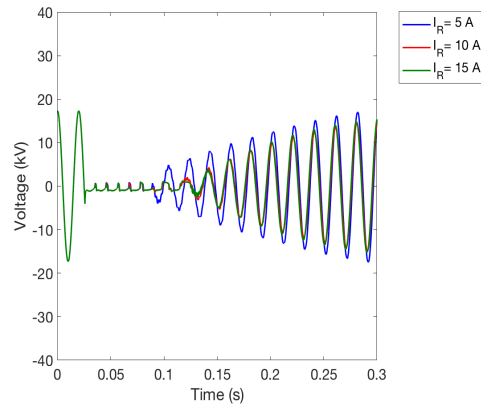


Figure 5.74: Fault voltages when detuning degree at +5% and fault inception at voltage zero-crossing

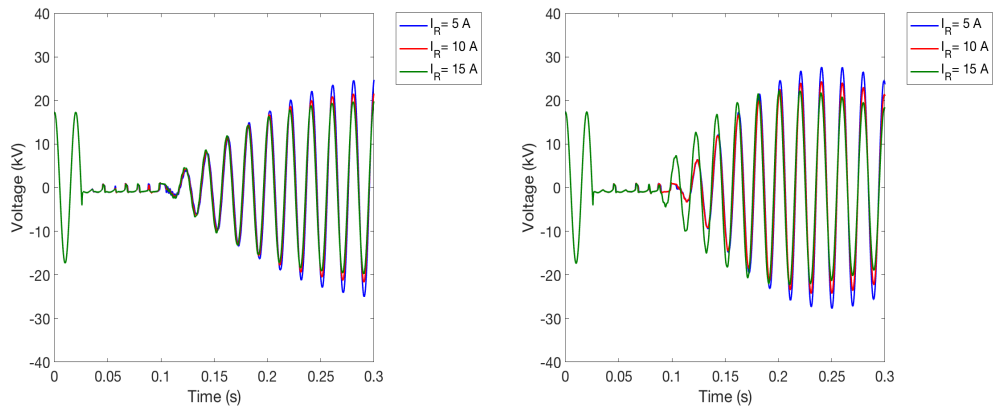


Figure 5.75: Fault voltages when detuning degree at +10% and fault inception at voltage zero-crossing

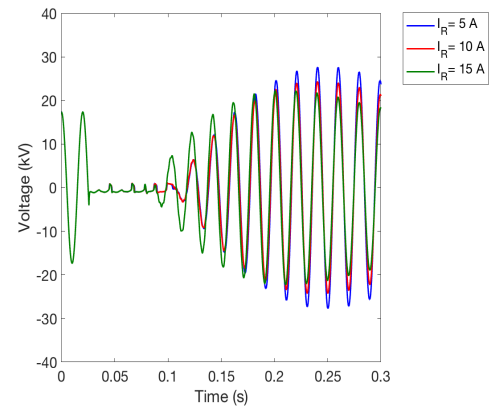


Figure 5.76: Fault voltages when detuning degree at +15% and fault inception at voltage zero-crossing

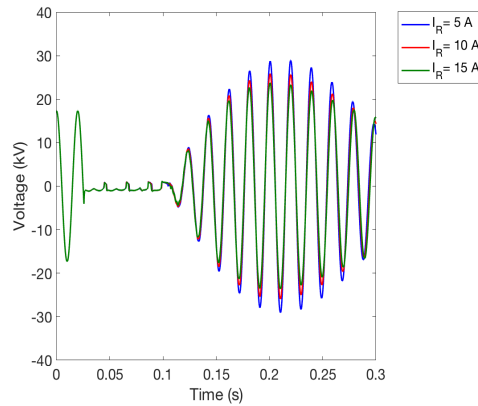


Figure 5.77: Fault voltages when detuning degree at +20% and fault inception at voltage zero-crossing

5.3.2.2 Arc current Measurements

Following section 5.3.2.1, figures 5.78 - 5.86 show the resulted arc currents while applying the exact testing conditions.

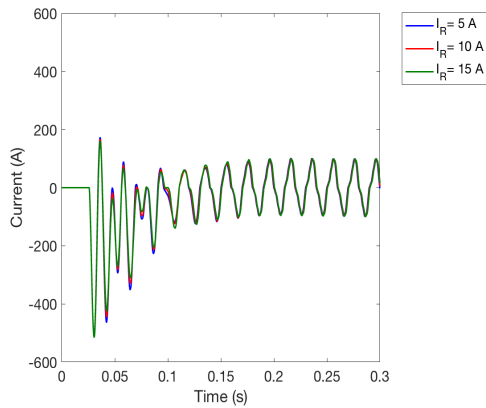


Figure 5.78: Fault currents when detuning degree at -20% and fault inception at voltage zero-crossing

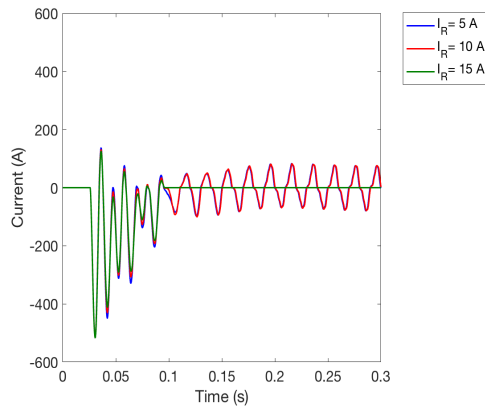


Figure 5.79: Fault currents when detuning degree at -15% and fault inception at voltage zero-crossing

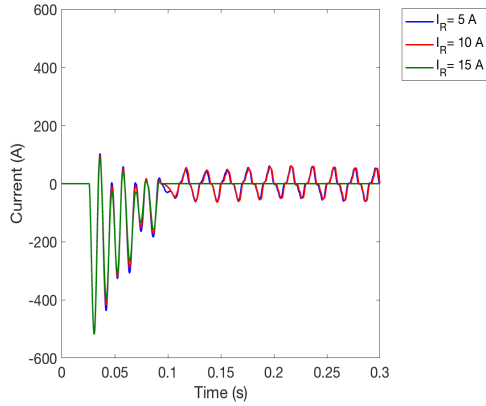


Figure 5.80: Fault currents when detuning degree at -10% and fault inception at voltage zero-crossing

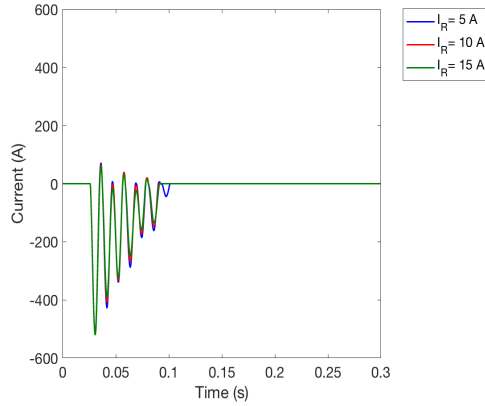


Figure 5.81: Fault currents when detuning degree at -5% and fault inception at voltage zero-crossing

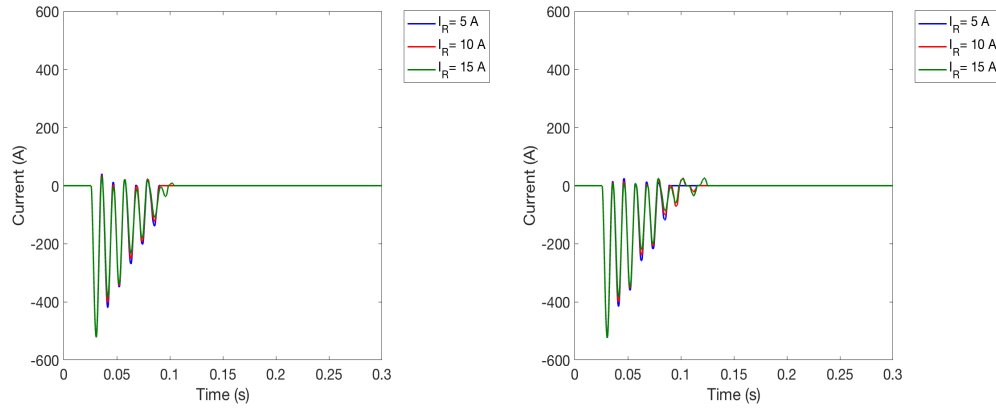


Figure 5.82: Fault currents when detuning degree at 0% and fault inception at voltage zero-crossing

Figure 5.83: Fault currents when detuning degree at +5% and fault inception at voltage zero-crossing

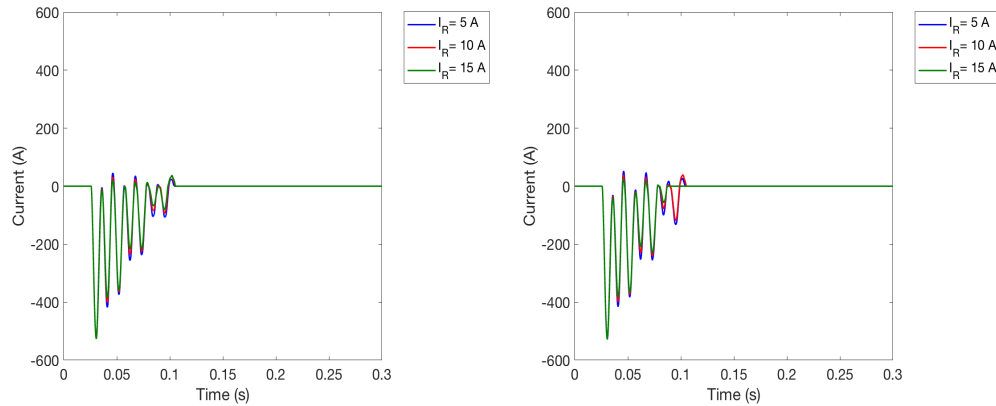


Figure 5.84: Fault currents when detuning degree at +10% and fault inception at voltage zero-crossing

Figure 5.85: Fault currents when detuning degree at +15% and fault inception at voltage zero-crossing

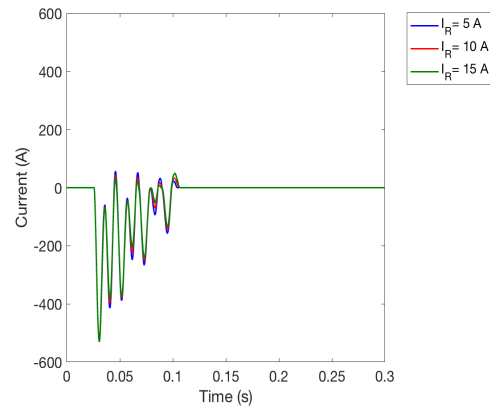


Figure 5.86: Fault currents when de-tuning degree at +20% and fault inception at voltage zero-crossing

Chapter 6

Discussion Based on Simulation Results

6.1 Arc Model Implementation Test

A comparison has been made between the obtained results and the results from [14]. It can be noticed that both results are similar which has led to the assumption that the system functionality has been confirmed for both tested scenarios.

6.2 The Effect of Detuning Petersen Coil Between -20% to +20%

The detuning of the Petersen coil has affected the arc current and voltage magnitudes. It has also affected the voltage waveform after the arc extinction. As been presented in table 4.1, at every detuning level, the value of the grounding coil changes. Increasing the detuning level towards the positive side will decrease the value of the grounding inductance. Thus, decreasing the DC and AC components in the arc fault current. On the other hand, decreasing the value of the detuning level towards the negative side increases the DC and AC components within the arc fault.

The time when the arc is self-extinguished was also effected by detuning grounding coils. The earliest arc self-extinguish time for both scenarios happens at 0%. For when the fault occurs at the maximum peak of the voltage, the arc current disappeared at $t = 0.087$ s and for the other scenario, arc extinguished at time $t = 0.102$ s. It can be noticed that when the percentage changes towards the positive or negative side, the time at which arc current is self-extinguished will increase.

6.3 The Effect of Implementing a Parallel Grounding Resistor

As previously mentioned in section 4.3, this study included two testing scenarios depending on the fault starting point. Either at the peak of the line voltage or zero-crossing point of the line voltage. The study was applied on several detuning levels from -20% to $+20\%$. This test also included three cases depending on the value of the parallel resistor, which are mentioned in table 4.2.

In both scenarios, the effect of implementing a parallel resistor in all three cases was not the same across all detuning levels. In general, the smaller is the active current I_R the higher is the arc voltage. This is directly proportioned to the total impedance value of the ground. It was noticed that the value of the parallel grounding resistor can also affect the arc self-extinction behavior. In one case, the arc would extinct earlier as when $I_R = 15$ A and the fault started at the voltage maximum peak while the detuning degree is -20% , i.e., figure 5.51. In that case, the parallel resistor has changed the arc current self-extinguish time to be $t = 0.073$ s compared to $t = 0.0998$ s when the system did not have a parallel resistor.

When comparing the effect of implementing a parallel grounding resistor to the arc self-extinction behavior in all three cases of I_R , it was noted that in some cases $I_R = 15$ A was the first to initiate the arc self-extinction as in figure 5.51 and 5.52. In other cases, $I_R = 5$ A was the first to initiate the arc self-extinction as in figure 5.53. Also, it was noticed that the self-extinction may start at the same time in all three cases of I_R .

Chapter 7

Conclusion

The thesis presented a mathematical model that can be used to simulate electrical arc faults in MV networks. The model has been verified by using real data from previous tests on an MV system that has resonant grounding. Furthermore, the system was used to study the effect of varying the detuning level of the Petersen coils. It was noticed that over or under detuning the coil has an effect on the AC and DC components of the arc fault. It was also noticed that detuning the coils can affect the self-extinguish behavior of the arc faults.

Another study has been conducted to see the effect of implementing a parallel grounding resistor with different set values to the Petersen coils. The parallel resistor has affected the self-extinction phenomena of the arc. This effect was not the same in all three studied cases of the parallel grounding resistor. Since it was noted that detuning the resonance coils at different levels could result in changing the relationship between the starting time of the arc self-extinction and the value of the parallel grounding resistor.

Bibliography

- [1] M Kizilcay and T Pniok. “Digital simulation of fault arcs in power systems”. In: *European Transactions on Electrical Power* 1.1 (1991), pp. 55–60.
- [2] Nagy I Elkalashy et al. “Modeling and experimental verification of high impedance arcing fault in medium voltage networks”. In: *IEEE Transactions on Dielectrics and Electrical Insulation* 14.2 (2007), pp. 375–383.
- [3] S Nitu et al. “Comparison between model and experiment in studying the electric arc”. In: *Journal of optoelectronics and advanced materials* 10.5 (2008), pp. 1192–1196.
- [4] Alireza Khakpour et al. “Electrical arc model based on physical parameters and power calculation”. In: *IEEE Transactions On Plasma Science* 43.8 (2015), pp. 2721–2729.
- [5] Toshiya Ohtaka, Viktor Kertész, and Rene Peter Paul Smeets. “Novel black-box arc model validated by high-voltage circuit breaker testing”. In: *IEEE Transactions on Power Delivery* 33.4 (2017), pp. 1835–1844.
- [6] AE Emanuel et al. “High impedance fault arcing on sandy soil in 15 kV distribution feeders: contributions to the evaluation of the low frequency spectrum”. In: *IEEE Transactions on Power Delivery* 5.2 (1990), pp. 676–686.
- [7] AR Sedighi and MR Haghifam. “Simulation of high impedance ground fault In electrical power distribution systems”. In: *2010 International Conference on Power System Technology*. IEEE. 2010, pp. 1–7.
- [8] M Aucoin, BD Russell, and CL Benner. “High impedance fault detection for industrial power systems”. In: *Conference Record of the IEEE Industry Applications Society Annual Meeting*, IEEE. 1989, pp. 1788–1792.

- [9] AM Sharat, LA Snider, and K Debnath. “A neural network based back error propagation relay algorithm for distribution system high impedance fault detection”. In: *1993 2nd International Conference on Advances in Power System Control, Operation and Management, APSCOM-93*. IET. 1993, pp. 613–620.
- [10] David Chan Tat Wai and Xia Yibin. “A novel technique for high impedance fault identification”. In: *IEEE Transactions on Power Delivery* 13.3 (1998), pp. 738–744.
- [11] TM Lai, LA Snider, and E Lo. “Wavelet transform based relay algorithm for the detection of stochastic high impedance faults”. In: *Electric power systems research* 76.8 (2006), pp. 626–633.
- [12] Yong Sheng and Steven M Rovnyak. “Decision tree-based methodology for high impedance fault detection”. In: *IEEE Transactions on Power Delivery* 19.2 (2004), pp. 533–536.
- [13] Marek Michalik et al. “Wavelet transform approach to high impedance fault detection in MV networks”. In: *2005 IEEE Russia Power Tech*. IEEE. 2005, pp. 1–7.
- [14] M Kizilcay and P Seta. “Digital simulation of fault arcs in medium-voltage distribution networks”. In: *Proceedings 15th Power Systems Computation Conference*. 2005, pp. 22–26.
- [15] M Kizilcay and T Pniok. “Digital simulation of fault arcs in power systems”. In: *European Transactions on Electrical Power* 1.1 (1991), pp. 55–60.
- [16] M Kizilcay and K-H Koch. “Numerical fault arc simulation based on power arc tests”. In: *European Transactions on Electrical Power* 4.3 (1994), pp. 177–185.
- [17] László Prikler et al. “Modeling secondary arc based on identification of arc parameters from staged fault test records”. In: *International journal of electrical power & energy systems* 25.8 (2003), pp. 581–589.
- [18] Christophe Prévé. *Protection of electrical networks*. John Wiley & Sons, 2013.
- [19] Maria Kättström. “Grounding of distribution grids: High impedance-grounding compared to solid grounding with Fault Current Limiter”. MA thesis. Uppsala University, conducted at ABB Corporate Research Center, 2017.

- [20] László Prikler and HK Hoidalen. “ATPdraw Version 5.6 for Windows 9x/NT/2000/XP/Vista-Users’ Manual”. In: *European EMTP ATP Users User Group* (2009).
- [21] Łukasz GRĄKOWSKI and Katarzyna GĘBCZYK. “Analysis of earth faults in the MV grid using the EMTP-ATP program”. In: *Przegląd Elektrotechniczny* 95 (2019).
- [22] László Prikler et al. “Improved secondary arc models based on identification of arc parameters from staged fault test records”. In: *14th PSCC*. 2002, pp. 1–6.
- [23] Laurent Dubé. “Users Guide to MODELS in ATP”. In: *Bonneville Power Administration* (1996).

